공학석사학위논문

Magnetite-Lithium Manganese Oxide Nanocomposite Having Lithium Adsorptive Properties in Aqueous Lithium Resource

수상의 리튬 자원에서 리튬 흡착능을 갖는
마그네타이트-리튬 산화 망간 나노복합체에 대한 연구

2014년 8월

서울대학교 대학원

재료공학부

오 승 희

ABSTRACT

Recently, the interest for lithium resources has been growing because the demand of lithium has been rapidly increasing as lithium secondary batteries become commonly used. Current lithium production is carried out mainly with brine of salt lakes and pegmatite, which are locally limited resources to particular countries. Although another lithium resource, seawater is highly accessible, since lithium ion in seawater exists at quite low concentration, 0.15-0.20 mg/L, the lithium recovery from seawater is considered ineffective and inefficient. However, the concentrated seawater undergone evaporative process to produce salt has enriched-lithium concentration and is expected to provide efficient and effective environment for lithium recovery system. Nevertheless, other cation enormously coexist in the lithium resource, requiring selective lithium extraction method to recovery lithium from the lithium resource.

Adsorption technique, the representative method to selectively extract lithium, has been investigated widely and considered as the appropriate technique for concentrated seawater due to its high selectivity to lithium and capacity. Among various adsorbents, the most prominent adsorbent, manganese oxide adsorbent can be prepared by extracting lithium from spinel-type lithium manganese oxide with acid treatment. Lithium recovery process using adsorbents includes several liquid-adsorbent separation process which several research groups have reported various type adsorbents, such as granulation and membrane, to enhance the efficiency of. However, these types of adsorbents require high manufacturing cost and the uses of harmful reagents. Therefore, it is necessary to develop other separation method which are

environmentally friendly and economically effective.

In this study, magnetically water-separable lithium adsorbent is suggested while realizing magnetite-lithium manganese oxide nanocomposite. To attain the material, primarily, spinel-type lithium manganese oxides (LMO) having different Li/Mn ratio, 0.63-1.00, were synthesized, which are the foundation where magnetite phase grows. Then, magnetite-LMO (M-LMO) was prepared by adding LMO in $Fe(OH)_2$ solution and heating the mixture in high temperature. With XRD and HR-TEM, it was found that two crystal phase exist on a particle of the product, and the mechanism of the reaction, Fe^{2+} redox reaction, was suggested based on the result of XPS and other related researches. On a basis of the proposed mechanism, several conditions were controlled to maximize magnetization and minimize the destruction of LMO during the reaction. With the optimized condition and LMOs having different Li/Mn ratio, M-LMOs were synthesized and the most effective LMO was determined with several lithium adsorption tests. As a result, the adsorbent from M-LMO of LMO-2.5 (M-LMO-2.5) showed higher lithium adsorbing capability, 6.84 mg/g which is 58.31% of the calculated capacity of LMO in the composite, and better stability for repetitive uses. Then, in order to certify the feasibility of M-LMO-2.5 for industrial application in concentrated seawater, the measurement of selectivity with distribution coefficient (K_d) and the adsorption tests in concentrated seawater were performed, and M-HMO showed high selectivity to lithium (K_d: $Li^+ >> Mg^{2+} > Na^+ > K^+$) and lithium adsorbing capability for the concentrated seawater, highly salty water. Consequently, the results of this study demonstrates that magnetite-lithium manganese oxide nanocomposite was successfully synthesized and could be a promising candidate as a magnetically water-separable and selectively lithium-adsorbable material for lithium recovery.

Keywords

Li ion recovery, Lithium manganese oxide, Magnetite, Composite, Adsorbent, Lithium resources

Student number: 2012-23148

CONTENTS

1. Introduction

Recently, a secondary batteries using lithium have been becoming more essential as many electronic devices, such as smart phone, hybrid or electronic vehicle and etc. adopt the secondary batteries for electronic source. Therefore, lithium grow to be more important element while the demand for lithium rapidly increase. According to estimation from U.S. department of energy, it is estimated that global lithium demand will become more than triple of the expected lithium global supply in 2015 before 2025 [1]. Thus, lithium reserves is likely exhausted in the near future, which could cause large increment in lithium price. In addition, as a possession of the resource become one of competence of a nation in global society, lithium plays an important role in global society and the exploitation of lithium resources turn out to be an issue over the world.

Since metallic lithium is chemically active in nature, lithium is produced from the mixture with other elements or chemical compounds. Lithium raw material exist in various forms in nature: brine in salt lake, pegmatite ores, sedimentary rocks and *etc.* Among them, brine is the most major resource of lithium, making up 66 % of world's lithium resources [2]. Brine is highly concentrated salt water including higher lithium concentration than other lithium resources, which leads to simple and low cost lithium production process. Generally, lithium is easily produced with evaporating brine water by the sun and refining the evaporated brine water. However, the brine water is locally restricted only in some specific districts or countries, such as Bolivia, Chile, Argentina, USA and China [2, 3]. Also pegmatite or sedimentary rocks including lithium component are limited only for some districts like Figure 2 [4]. Therefore, other countries which do not have brine or pegmatite are searching for new lithium resources able to

substitute conventional lithium supplying sources. As the new lithium resources, there are geothermal water and seawater. Geothermal water is the ejected water from geothermal power plant where lithium exist in approximate 10 mg/L concentration. This is a feasible resource to produce lithium, but it is also locally limited because the required states for geothermal power generation are pretty conditional. Seawater is other new lithium resources which attracts global attention recently. Since its accessibility is pretty higher than other resources and it has considerable deposition amount of lithium, totally 230 billion tons, many countries having coast or ocean are developing lithium extracting technology due to its feasibility. However, lithium concentration in seawater is 0.1 mg/L to 0.2 mg/L, which is too low concentration to adopt conventional lithium production method in brine, evaporating and refining production process. Because of a large amount of other cation, such as sodium, potassium, magnesium and calcium coexisting in seawater, its cost and energy to separate and refine lithium using evaporating method is quite high and thus, the method is not proper method for extract lithium from seawater. Therefore, in order to acquire feasibility of lithium production from seawater at an industrial level, the method able to selectively extract lithium from seawater without using a lot of energy and high cost is indispensable.

There are several methods which can extract lithium ion from aqueous lithium resources and recovery the lithium ion: adsorption (ion-exchange) [5-10], solvent extraction [11-12] and co-precipitation [13]. These technologies have been investigated for various aqueous type lithium resources and among them, the adsorption method is considered as the most suitable lithium extraction method for aqueous lithium resources, such as seawater, due to its extremely high selectivity for lithium ion. Since the

mechanism of the method is described by the presence of micropores in the adsorbent crystal, which is suitable size for passing small lithium ion and excluding other large size cation, the method is called by ion-sieve type adsorption method. The method uses inorganic adsorbent having ion-exchange properties for lithium ion and is operated in batch-type process, which require low cost industrial infrastructure. While vast studies on the inorganic adsorbent have been done, many different kinds of adsorbents have been developed for the extraction of lithium: HMn_2O_4, $HSbO_3$, H_2TiO_3, $HZr_2(PO_4)_3$ [14-17]. Among these inorganic adsorbents, manganese oxide-based adsorbent have been recognized as the most interesting adsorbent due to its higher selectivity and capacity to lithium ion than others, and environmentally harmlessness and low cost. The manganese-based adsorbent could be generated from spinel-type lithium manganese oxide after extracting lithium from spinel structure. In addition to its application for adsorbent of lithium, spinel-type lithium manganese oxide has been developed for cathode material of lithium secondary batteries and electrode for selective electroinsertion of Li ion [18] due to its selective lithium adsorption properties. There are many kinds of lithium manganese oxide existing because in spinel framework manganese can take the trivalent and tetravalent states and lithium content can vary. According to Figure 3 summarized by an earlier work [19], lithium manganese oxide phase could be varied by Li/Mn ratio, the valence state of manganese and exchanged lithium content amount. Among these manganese oxide, spinel-structure $LiMn_2O_4$, $Li_{1.33}Mn_{1.67}O_4$, $Li_{1.6}Mn_{1.6}O_4$ have attracted lots of attention and many research group have reported many studies about these materials [19-21]

Spinel type-lithium manganese oxide is the crystal framework based

on cubic closed packed structure constructed oxygen atoms. In case of a typical spinel-type lithium manganese oxide, $LiMn_2O_4$, manganese (III) and manganese (IV) atoms are located in 16d octahedral sites, occupying half octahedral sites and composing Mn-O octahedron structure with oxygen atoms, and lithium atoms occupy 8a tetrahedral sites. As lithium content increase in the spinel structure, extra lithium occupies the Manganese octahedron sites, which raise the manganese valence state close to 4.0 and stabilize the spinel crystal structure. Therefore, there are two representative spinel lithium manganese oxide, $LiMn_2O_4$ and $Li_{1.33}Mn_{1.67}O_4$, the former is consist of Mn (IV) and Mn(III) equally and the latter one is composed only with Mn (IV). And spinel lithium-rich manganese oxide, $Li_{1.6}Mn_{1.6}O_4$ [21] is reported as a cation-deficient lithium manganese oxide having hexagonal lattice having only Mn (IV). Lithium desertion from these spinel type lithium manganese oxide, $LiMn_2O_4$, $Li_{1.33}Mn_{1.67}O_4$, $Li_{1.6}Mn_{1.6}O_4$ lead to derive spinel-type manganese oxide having proton lattice, λ-MnO_2, MnO_2 ·0.31H2O, MnO_2 ·0.5H_2O respectively which have selective lithium adsorption properties.

Lithium desertion process is carried out with acid treating lithium manganese oxide. The lithium-extracted manganese oxide can selectively adsorb and insert lithium ion with protonated spinel crystal framework. The lithium desertion/insertion process of the spinel lithium manganese oxide in aqueous solution have been studied by many research groups [5-10, 19-21] and the process are expressed with the following reactions.

Li desertion process

Ion-exchange-type reaction:

$$LiMn_2O_4 + H^+ \rightarrow HMn_2O_4 + Li^+$$

Redox-type reaction:

$$LiMn_2O_4 + 2H^+ \rightarrow Li^+ + (1/2)Mn^{2+} + H_2O + Mn_{1.5}O_3$$

Li Insertion process

Ion-exchange-type reaction:

$$HMn_2O_4 + Li^+ \rightarrow LiMn_2O_4 + H^+$$

Redox-type reaction:

$$HMn_2O_4 + Li^+ + OH^- \rightarrow LiMn_2O_4 + (1/2)H_2O + (1/4)O_2$$

These reactions had been proposed and investigated by many researchers [19, 22-23] and the mechanism was completed by defining two kinds of sites for lithium: redox-type and ion-exchange-type, and the proportion of each type can be varied according to the spinel type lithium manganese oxide characteristics, such as Li/Mn ratio and the valence state of Mn [20]. These reaction is well described in Figure 4 which was proposed by a researching group [20]. Through these reactions, lithium is extracted from lithium manganese oxide crystal and the lithium-extracted manganese oxide, λ-MnO_2 or HMn_2O_4 can insert lithium ion into its spinel framework. Then, the reversible lithium desertion and insertion process can be developed into a lithium recovery system from lithium aqueous sources. According to the above reactions, while redox-type reaction progress in acid solution, manganese dissolution in crystal occurs. As the typical spinel type $LiMn_2O_4$ is described in the reaction, Mn(III) coexisting with Mn(IV) in lithium manganese oxide undergo redox reaction. Some portion of Mn(III) turn into Mn(IV) with oxidization and other portion become Mn(II) with reduction, which cause the dissolution of lithium manganese oxide crystal. Therefore,

the dissolution of manganese during acid treatment of lithium manganese oxide can be minimized by reducing the portion of Mn(III) and developing ion-exchange-type reaction in desertion process dominantly. In the desertion process of $Li_{1.33}Mn_{1.67}O_4$ and $Li_{1.6}Mn_{1.6}O_4$ formed with 100 % tetravalent manganese, lithium extraction is dominantly advanced by ion-exchange-type reaction and a small portion is progressed by redox-type reaction, which endow the lithium manganese oxides with a high chemical stability against whole process of lithium desertion/insertion process. And it is expected that those ion-exchange-type lithium manganese oxides have the significant large lithium adsorption capacity on the basis of the higher lithium content of those crystals in chemical composition [21].

Due to these advantages, the $Li_{1.33}Mn_{1.67}O_4$ and $Li_{1.6}Mn_{1.6}O_4$ have been broadly investigated for the structural and chemical characteristics and the preparation method, such as a sol-gel method, sold-state method and hydrothermal method [7-8, 24-25]. Also, the investigations for the actual application in industrial levels have been done by several research groups. These research groups applied the adsorbents in powder condition for various lithium aqueous sources, seawater, brine and geothermal water [9, 26-28]. However, powder form of adsorbent have limitation for its industrial application because separation process from liquid medium is necessary in a batch-type system described in Figure 5 and the powder form is recognized having low efficiency for separation process. In order to overcome this limitation, several research groups have been studying the introduction of other material with the inorganic adsorbents and the change of the form of the inorganic adsorbents. Most studies have been dealt by achieving granulation and membranization using inorganic lithium adsorbent, lithium manganese oxide. Macroporous silica bead [29], macroporous cellulose gel

bead [30], polyvinyl chloride (PVC) [28, 31] were implemented to realize granulation and applicable size lithium adsorbents. The other research groups had reported foam-type lithium adsorbents by using various binders, such as pitch [32] or agar [33], with lithium manganese oxide as a precursor. These granulations and form-types of lithium adsorbent were converged to use column operation system for lithium recovery, which is more convenient, but it requires large pressure and high energy consumption. Therefore, other research groups have studied membrane-type lithium adsorbing system to avoid column operation system which require a high pressure. Firstly it was reported membrane-type lithium adsorbent prepared by impregnating $Li_{1.33}Mn_{1.67}O_4$ into PVC in N,N-dimethylformaide (DMF) [34]. In addition, other groups have reported other forms membrane-type lithium adsorbent, flat sheet form [35], polymeric reservoir form like tea bag figure [36] on a basis of PVC as a binder, DMF as a solvent and spinel-type lithium manganese oxide as a precursor. These membrane-type lithium adsorbent might be suitable because of its applicability for continuous operation system, but the fabrication of these membrane requires high manufacturing cost and the uses of a large amount of environmentally harmful reagents, and generate massive DMF wastewater which is a highly-toxic substance for humans. Therefore, it is necessary to develop new selectively lithium adsorbable material conducting other form lithium recovery system for industrial applications and overcoming the disadvantages of the granulation-type and the membrane-type lithium adsorbent. As another form of recovery system, there is a magnetically adsorbent-separable system. This system is using magnetic particles having a particular function for a specific purpose in liquid medium, which is able to be separated from liquid medium by applying a magnetic field. The system has been investigated by many

research groups in other field, such as the harmful substance removal system in aqueous medium. However, in lithium recovery filed, this has hardly ever been researched. In this system operated in a batch-type, the magnetic particle showing specific functions is the core material for operation, which is mainly derived from magnetic material by realizing composite with other material.

As a representative magnetic material, there is magnetite, Fe_3O_4, one of conventional iron oxide. Unlike other conventional iron oxide, hematite and maghemite, magnetite is composed by two kinds of iron elements, Fe(II) and Fe(III) distributed in inverse spinel structure of oxygen-cubic closed packed framework. This iron oxide shows ferrimagnetic property in bulk state, but it turn out to be superparagmagnetic property when the state of iron oxide become nanoparticle scale. Magnetite nanoparticle behave like a paramagnetic atom having large magnetism, which can rapidly response to applied magnetic fields with small remnant magnetism and coercivity. In addition, since magnetite has high curie temperature and low blocking temperature, its magnetic properties is thermally stable and able to be maintained in a wide temperature range. These characteristics of magnetite nanoparticle are desirable for actual application, such as environmental remediation, biomedical application and other various field. The iron oxide, Fe_3O_4 not only shows high biocompatibility and low toxicity in the human body [37-38], but also is environmentally harmless material. Therefore, their applications in environmental field, such as water treatment are considered appropriate and already many research groups have studied these aspects of magnetite [39-41]. Also because of its inexpensive reagents for preparation and various synthetic methods, magnetite nanoparticle can be easily and affordably prepared. For the industrial applications or other purposes, many

research groups hsave tried to endow a particular function to magnetite with functionalization of magnetite surface by organic or inorganic material. Organic compounds are employed for various purposes like passivation of magnetite, improvement of biocompatibility and other specific application. Besides organic materials, inorganic compounds are used for functionalization of magnetite by forming various structure composites. The main purposes of functionalization of inorganic compounds can approximately be divided into two categories: introduction of magnetic properties and introduction of inorganic material properties. Depending on the researching purposes, various inorganic compound, such as silica, metal or oxides, are utilized and many skillful approaches have been investigated to successfully hybrid two materials. In addition to these aspects, many studies have been done in order to control the nanostructure of composite. In Figure 6 summarized by Wei Wu *et al.,* the structure of nanocomposite can roughly divided into five types: core-shell, mosaic, shell-core, shell-core-shell and dumbbell [42]. Most studies have dealt with the already prepared magnetic nanoparticle for forming nanostructured composite and not much studies were focused on the nanostructure constructed by the growth of magnetite on the surface of inorganic materials.

In this study, magnetically water-separable and selectively lithium-adsorbable nanocomposite was prepared using the cost-effective and environmentally friendly method, and several experiments were carried out to find more effective and proper fabrication method for the magnetite-lithium manganese oxide. Firstly, lithium manganese oxides varied with lithium content in the phase were synthesized to verify those lithium adsorbing capability and find proper candidate precursor for magnetite-lithium manganese oxide composite. Then, onto the synthesized lithium

manganese oxides, the magnetite phase was constructed by reacting the lithium manganese oxide with $Fe(OH)_2$ and hydrothermal reaction, and magnetite-lithium manganese oxide composite was formed. On a basis of the mechanism derived from the analyses results, several experiments were performed to adjust magnetization and lithium adsorbing properties of the composite. Then, the optimized fabrication method for the composite was prepared. In order to find the most proper lithium manganese oxide as a precursor for composite, magnetite-lithium manganese oxides from the lithium manganese oxides having different properties were prepared and characterized with several analyses, XRD, VSM, chemical composition analysis, and BET. Then, through lithium adsorption tests and repetitive adsorption tests using adsorbents from each magnetite-lithium manganese oxides, the most appropriate composite was selected. The applicability of the selected composite for actual lithium recovery system was investigated by measuring its selectivity to lithium and performing the adsorption test in a possible lithium aqueous resource, concentrated seawater. Concentrated seawater is the highly salty water from the seawater treated with evaporative process. As one of lithium resources, seawater is not an effective resource due to its pretty low lithium concentration, 0.15~0.20 mg/L. However, it is a very important lithium resource for several countries because of its high accessibility compared with other resources. As a refined version of seawater, the concentrated seawater is suggested as more effective and efficient lithium resources having approximately 0.8-3.2 mg/L lithium concentration. Therefore, the lithium recovery system built by using the lithium resource could provide more effective foundation for lithium production industry.

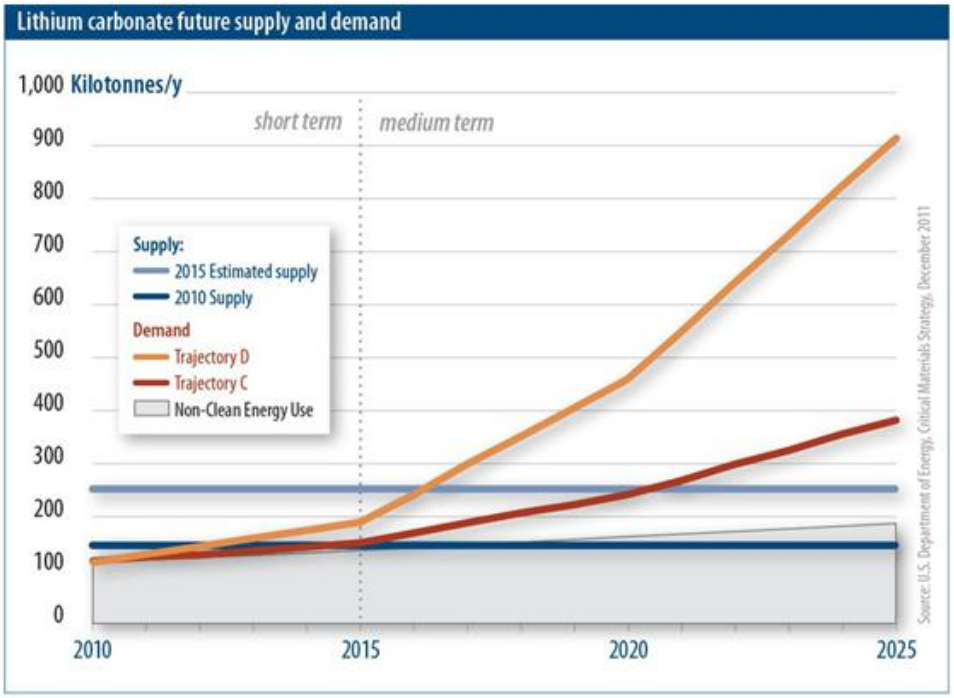

Figure 1. Estimation of future lithium demand and supply from U.S. DOE. [1]

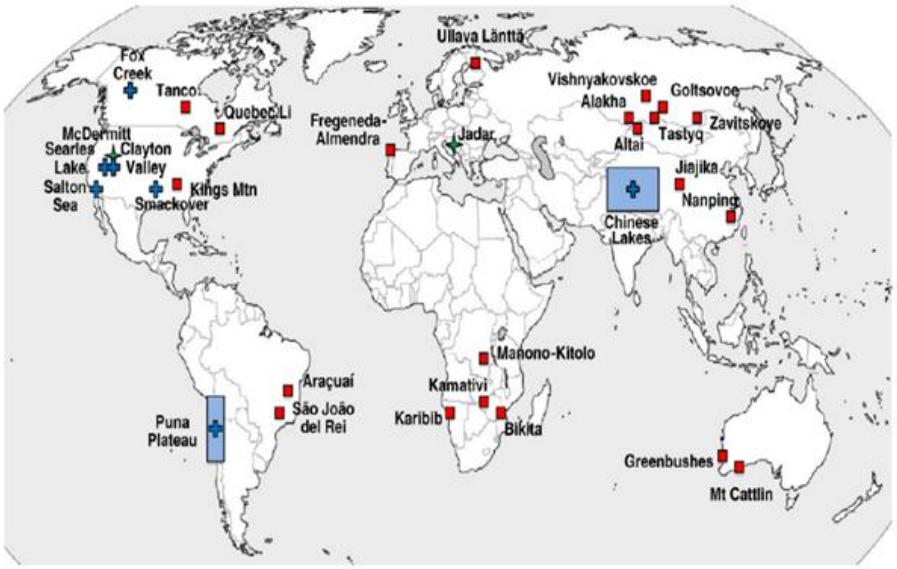

Figure 2. Location of lithium resources, pegmatite (square) and brine (cross) deposits referred from the previous work [4]

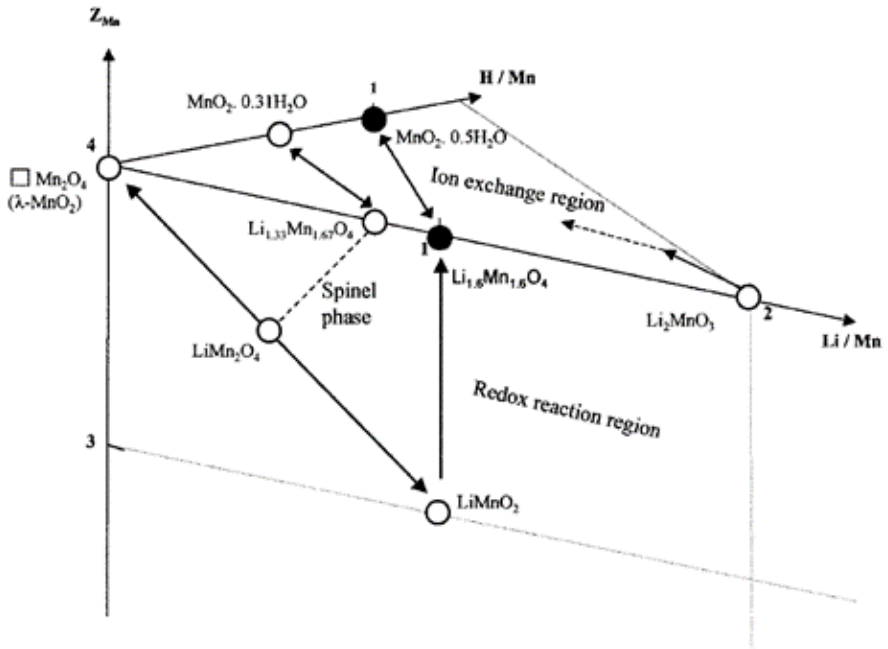

Figure 3. Phase diagram of lithium manganese oxides and their lithium-extracted forms summarized from the previous work [19]

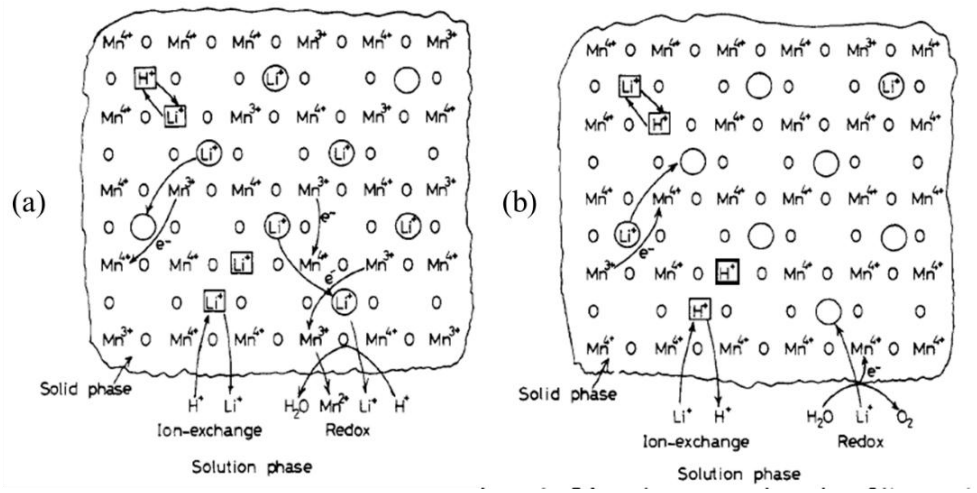

Figure 4. Schematic diagram of Li+ desertion reaction, (a), and Li+ insertion reaction, (b), described from the previous work [20]

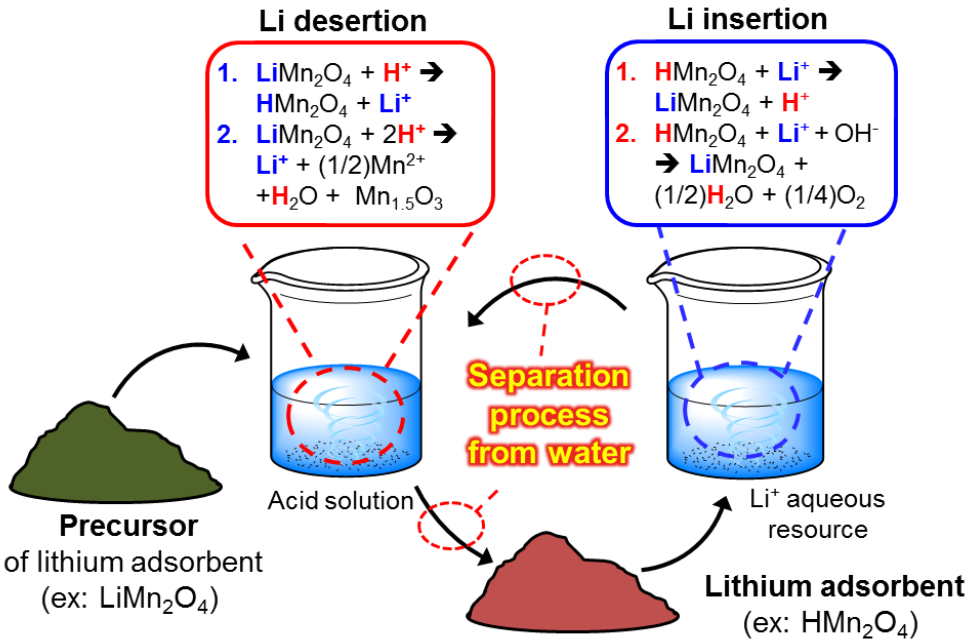

Figure 5. Description of lithium recovery process using powder-type adsorbent

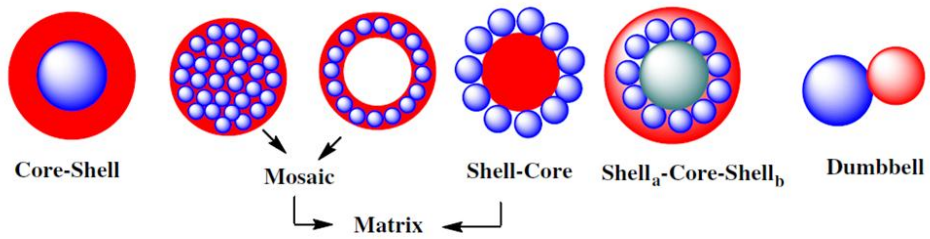

Figure 6**. The main structures of inorganic composites with magnetic iron oxide nanoparticles summarized by the previous work [42]**

2. Experimental section

2.1 Materials

Manganese sulfate monohydrate ($MnSO_4 \cdot H_2O$, DAEJUNG), lithium hydroxide monohydrate ($LiOH \cdot H_2O$, JUNSEI) and hydrogen peroxide (H_2O_2, 30%, JUNSEI) were used as the reagents for the spinel structure lithium manganese oxide. Iron(II) sulfate heptahydrate ($FeSO_4 \cdot 7H2O$, 99+%, Sigma-Aldrich) and sodium hydroxide, pellet (NaOH, DAEJUNG) were used to make ferrous hydroxide which was used as the precursor for magnetite-lithium manganese oxide composite. As the additives for preparing of the composite, sodium acetate anhydrous ($C_2H_3O_2Na$, Sigma-Aldrich) and L-glutamic acid ($C_5H_9NO_4$, 99.0%, SAMJUN) are employed. Hydrochloric acid (HCl, 35%, DAEJUNG) was used for diluted hydrochloric acid. In the redox titration experiment of lithium manganese oxide, Iron(II) chloride tetrahydrate ($FeCl_2 \cdot 4H_2O$, Sigma-Aldrich) and potassium permanganate ($KMnO_4$, JUNSEI) were used as reducing and oxidizing agent. All chemicals were used as received without any further purification. Highly deionized water with resistivity of 18.0 $M\Omega \cdot cm^{-1}$ was used during the whole experiments.

2.2 Preparation of spinel structure lithium manganese oxide (LMO)

Lithium manganese oxide having spinel structure was synthesized with hydrothermal method referring to the previous work [8]. Lithium precursor solution was prepared by dissolving $LiOH \cdot H_2O$ and H_2O_2 (30%) in deionized water. 0.4 M $MnSO_4 \cdot H_2O$ solution was prepared in Teflon-lined stainless steel autoclave. 50 mL LiOH and H_2O_2 solution was dropped into 50 mL 0.4 $MnSO_4$ solution stirred with magnetic stirring. After maintaining this mixture with stirring for 2 h, the autoclave was sealed and then heated at 110 °C for 8 h. After cooled the autoclave to room temperature, the precipitate was filtrated and washed with deionized water for several times. And the obtained precipitated was dried at 60 °C for at least 12 h and calcinated at 400 °C for 4 h. In order to obtain lithium manganese oxide having various Li/Mn ratio, LiOH precursor amount was varied from 1.0 M to 3.0 M and the samples were designated as LMO-1.0 to 3.0, respectively. This method is described in Figure 8.

2.3 Preparation of magnetite-lithium manganese oxide (M-LMO) composite

The composite was synthesized with developing magnetite crystal on the surface of LMO. Firstly, 1.6 g $FeCl_2 \cdot 4H_2O$ and additive (sodium acetate, glutamic acid, no additive) were dissolved in deionized and deoxygenated water (30, 60, 90 mL). And 40 % NaOH solution (3, 4.5, 6 mL) was dropped into $FeCl_2$ solution with magnetic stirring and kept for 30 min to form greenish-white $Fe(OH)_2$ solution entirely. The precipitation process of

$Fe(OH)_2$ was carried out under nitrogen gas to maintain deoxygenated conditions. Then, LMO solution which was prepared by adding and dispersing LMO into 20 mL deionized water was added in $Fe(OH)_2$ solution. While magnetic stirring under N_2 atmosphere, the mixture was maintained in room temperature for 1 h. The mixture was transferred to Teflon-lined stainless steel autoclave and heated at 200 °C for 12 h. After cooled naturally, the magnetic powder was separated with a magnet and washed with deionized water, and the process was repeated for several times. And the powder was dried in 60 °C for 12 h. By adjusting the reaction conditions of solvent volume, additive, the amount of NaOH (40 %) solution and LMOs, the effect of each conditions for synthesizing the composite was clarified and the optimized composite was produced based on those effects. The whole process is depicted in Figure 8.

2.4 Acid treatment for Li^+ extraction from LMO or M-LMO

In order to give lithium adsorption property to LMOs or M-LMOs, lithium extraction process was carried out with acid treatment. LMOs or M-LMOs were immersed in 0.5 M HCl solution and shaken with 150 rpm for 24 h. The acid-treated samples were separate from HCl solution and washed with deionized water for several times and dried at 60 °C. Each samples are designated as HMOs and M-HMOs, respectively.

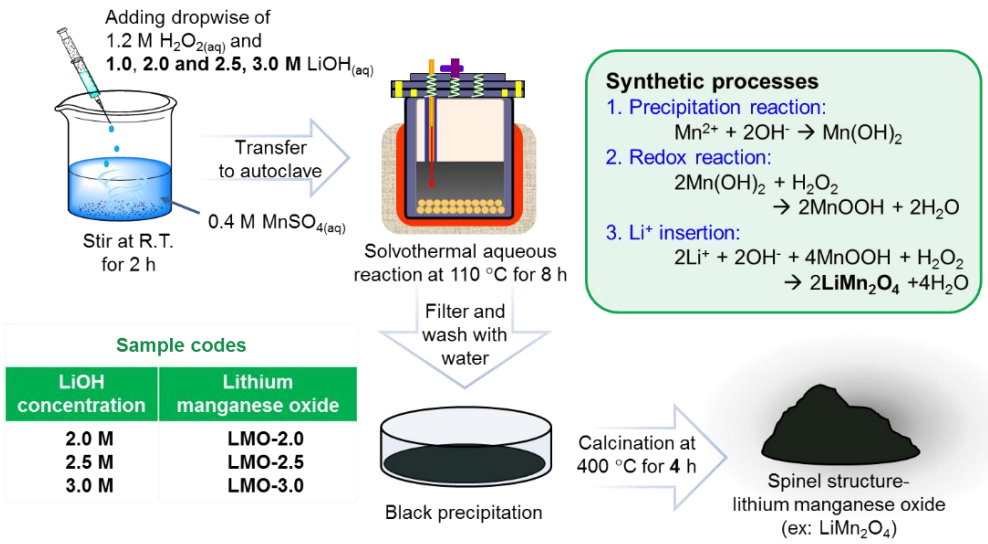

Figure 7. Scheme for synthesis of lithium manganese oxide (LMO) varied with lithium precursor amount

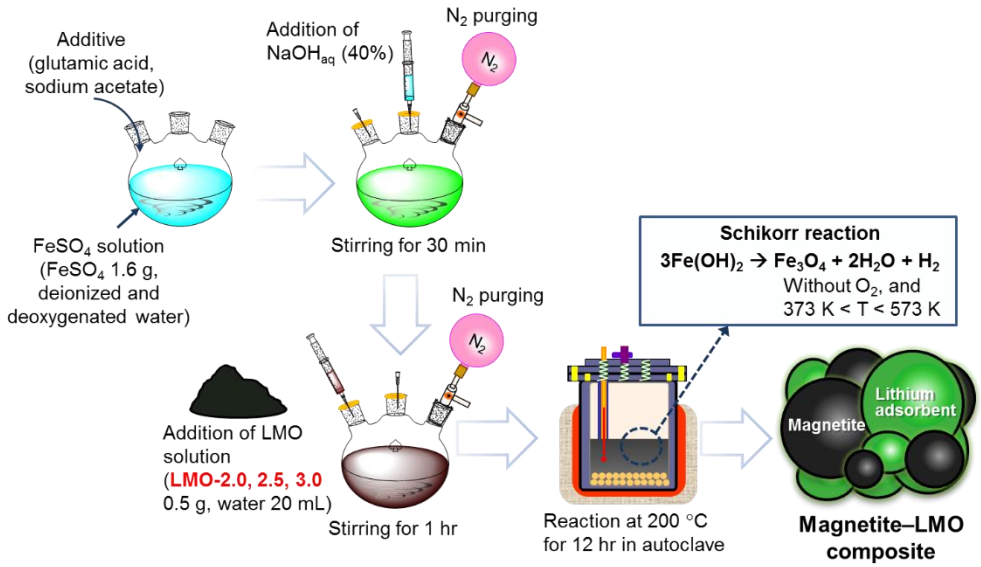

Figure 8. Scheme for preparation method of magnetite-lithium manganese oxide (M-LMO)

Adjustment	Dispersity	Schikorr reaction condition	Size of magnetite phase	LMO precursor
Condition	Solvent volume	Additive type	40% $NaOH_{aq}$ amount	LMOs
Variation	30 mL 60 mL 90 mL	Acetate Glutamate	3.0 mL 4.5 mL 6.0 mL	LMO-2.0 LMO-2.5 LMO-3.0

Table 1. Synthesized M-LMO from various conditions

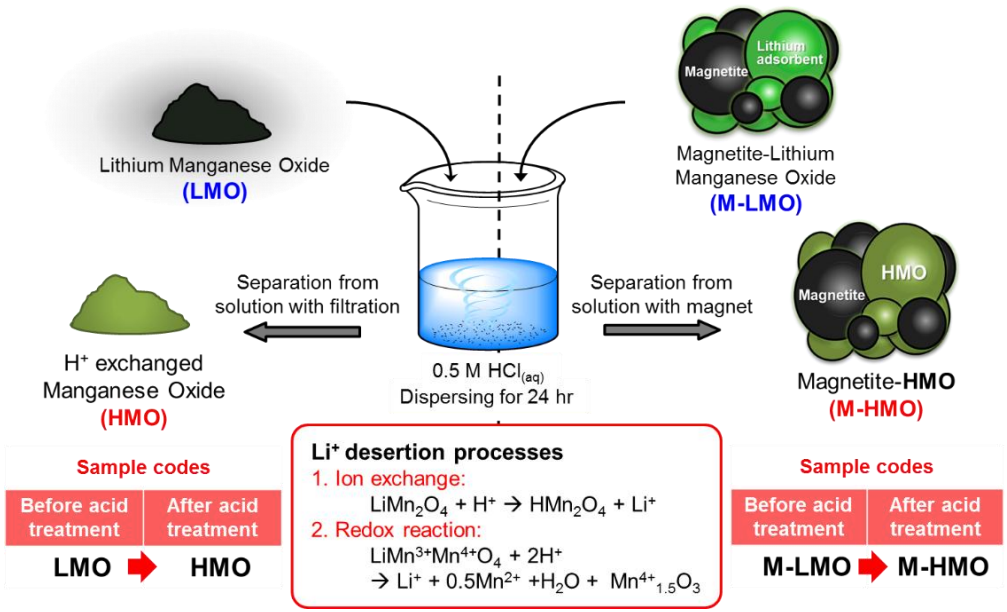

Figure 9. Lithium desertion from LMO and M-LMO turning into HMO and M-HMO after acid treatment

2.5 Characterization

2.5.1 Physical analysis of lithium manganese oxide (LMO) and magnetite-lithium manganese oxide composite (M-LMO)

The synthesized lithium manganese oxide (LMO) and magnetite-lithium manganese oxide composite (M-LMO) were characterized by the following physical analyzing method. In order to identify and compare the crystal phases of LMO and M-LMO, powder X-ray diffraction (XRD) was carried out using Bruker New D8 Advance X-ray diffractometer with Cu Ka radiation (a = 1.5406 A, 40 KV, 40mA), scanning from 10 to 80 at the speed of 10 degree per second. According to parameters obtained from XRD results and Debye-Scherrer equation, $D = K\lambda/\beta\cos\theta$, the average crystallite size of LMO was calculated. In Debye-Scherrer equation, D means the crystallite size of a specific peak, λ is the wavelength of X-ray irradiation, K is a constant related with the shape of crystal and usually assumed as 0.89, β is the full width at half-maximum intensity (FWHM) of a specific peak obtained from XRD and θ is the diffraction angle of the specific peak of LMO. The morphologies and crystallography were observed using high resolution transmission electron microscopy (HR-TEM) on a JEOL JEM-3000F at accelerating voltage of 300 KV after LMO or M-LMO were dispersed in ethanol with ultrasonic for 5 min and sampled onto the Formvar-stabilized Cu grid for observation. The specific surface areas were calculated with the Brunauer-Emmett-Teller (BET) equation using Micrometrics ASAP 2010 BET. In the case of M-LMO, magnetic properties were measured by a vibrating sample magnetometry (VSM) for the dried powders at the room temperature in the range of ±10 KOe magnetic field.

2.5.2 Chemical analysis of lithium manganese oxide (LMO) and magnetite-lithium manganese oxide composite (M-LMO)

The following chemical analysis were done for the LMO and M-LMO samples, respectively. Compositional analysis of LMO or M-LMO were carried out by fully dissolving LMO or M-LMO in hydrochloric acid solution containing peroxide and the lithium, manganese and iron contents in the solution were measured with VARIAN 730ES inductively coupled plasma (ICP) emission spectrometer. For the synthesized LMO samples, the mean oxidation number of manganese (Z_{Mn}) was estimated from the available oxygen determined from the redox titration using potassium permanganate solution. X-ray photoelectron spectroscopy (XPS) were performed to measure the electronic and chemical states of Fe and Mn in LMO and M-LMO using KRATOS AXIS-His with monochromatic Mg Kα radiation as X-ray source. All of the raw data were adjusted for calibrating and locating the C1s peak on the 284.5 eV binding energy.

2.6. Evaluation of adsorptive properties of lithium manganese oxide (LMO) and magnetite-lithium manganese oxide composite (M-LMO)

2.6.1 Lithium ion adsorption isotherm test of LMO and M-LMO in batch system

Lithium ion adsorption isotherm and equilibrium test was carried out with the prepared lithium solution in laboratory. Lithium solution was prepared by dissolving LiCl in deionized water at 0.01 M Li^+ (69.4 mg/L). The buffer solution (0.2 M ammonium hydroxide/ammonium chloride solution)

was added into the 0.01 M lithium solution for adjusting pH of the solution to 10.10. For a batch system experiment, all test was conducted by using 125 mL vial containing lithium solution. Lithium adsorbents (acid treated LMO or M-LMO) was added into 0.01 M lithium solution in 1.0 g/L concentration (100 mg adsorbent in 100 mL lithium solution). The vial containing the mixture was shaken for about 72 h at 298 K. Then, in order to separate adsorbent from sorbent, in case of the adsorbent from LMO, the mixture was centrifuged but, for the adsorbent from M-LMO, it is separated by applying external magnetic field using magnet. The lithium concentration of remaining solution was measured with inductively coupled plasma (ICP) emission spectrometer. The lithium ion adsorption capacity per gram of adsorbent (Q_e) was calculated from the change of lithium concentration after adsorption test to the following equation:

$$Q_e = (C_0-C_e)V/W$$

in which Q_e is the amount of adsorbed lithium ion per gram of adsorbent at equilibrium (mg/g), C_0 is the initial concentration of lithium solution (mg/L), C_e is the concentration of remained lithium solution at equilibrium (mg/L), V is the solution volume (mL) and W is the weight of adsorbent (g).

2.6.2 Repetitive lithium ion adsorption test of M-LMO

Repetitive lithium ion adsorption isotherm and equilibrium test was conducted only for the adsorbents from M-LMO. After lithium ion adsorption test, the separated adsorbent was dried at 60 °C and immersed in 0.5 M HCl solution and shaken for 24 h in order to regenerate the adsorption property. Then, separated adsorbent from HCl solution was washed with deionized water several times and dried at 60 °C. For the regenerated adsorbents, lithium ion adsorption test was conducted in the same condition of the first test and lithium ion adsorption capacity was measured. This process was repeated for 2 times.

2.6.3 Measurement of selectivity of lithium ion compared to other cation for M-HMO

The selectivity of adsorbent, M-HMO for Li^+ to other cation, Na^+, K^+, and Mg^{2+} mainly coexisting in seawater was evaluated by comparing distribution coefficient (K_d) for each ions. The distribution coefficient typically is employed as an index for how much an adsorbent is liable to adsorb a specific and individual adsorbate in a particular media. This coefficient can be measured by the ratio of the amount of the adsorbed adsorbate per unit mass of adsorbent to the amount of the remaining adsorbate in solution. Therefore, K_d value was determined by dispersing 0.1 g adsorbent, M-LMO, in 10 mL solution containing about 0.01 M of several cation, Li^+, Na^+, K^+, and Mg^{2+} at pH 10.10, respectively, and shaking the vial containing the solution to maintain dispersity of adsorbent in solution for 72 h at 298 K.

After reaching the equilibrium, the remained solution was analyzed with inductively coupled plasma (ICP) emission spectrometer to measure each cation concentration. Then, the K_d value for each cation was determined on the basis of the measured cation concentration and the following equation.

K_d (mL/g) = Adsorbed cation ion per a gram of adsorbent, M-LMO (mg/g)
/Cation ion concentration in remained solution (mg/mL)

2.6.4 Lithium adsorption test of M-HMO in the concentrated seawater

For verifying the feasibility of industrial application for the prepared M-HMO, lithium adsorption test was carried out in one of actual lithium resources, concentrated seawater. Concentrated seawater, as mentioned in introduction section, is the seawater which undergone the evaporative process and have higher lithium concentration than regular seawater. The content of each cation are shown in Table 2. Lithium adsorbent, M-HMO, was immersed in concentrated seawater with 0.1 g/L adsorbent concentration and stirred with mechanical stirrer for 5 days at the room temperature. Then, after separating magnetic M-HMO particle with magnet, the remained seawater was sampled and analyzed with ICP.

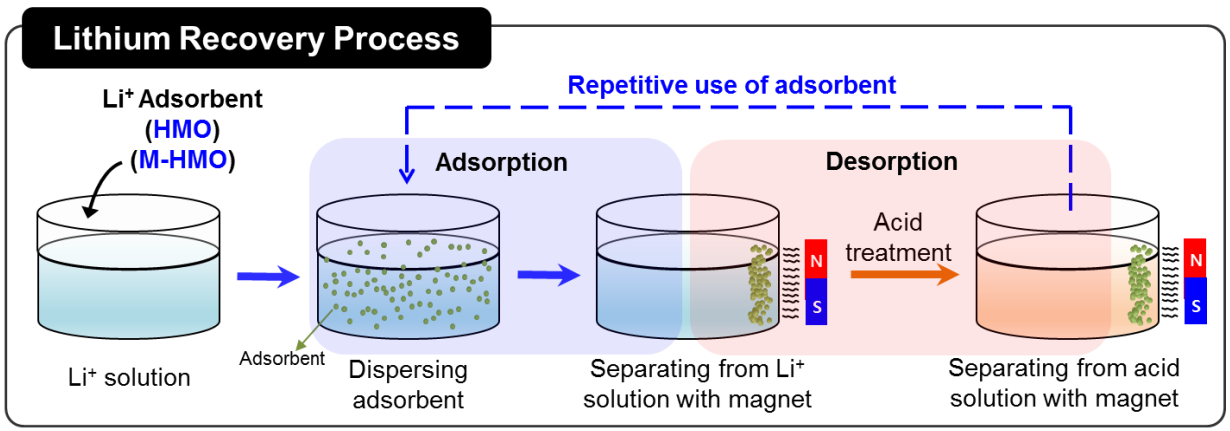

Figure 10. Schematic process of lithium adsorption and repetitive tests of M-HM

Element	Lithium Aqueous Resources	
	Seawater	Concentrated Seawater
Li^+	0.15-0.20 mg/L	0.8 mg/L
Na^+	10,900 mg/L	71,750 mg/L
K^+	390 mg/L	8,750 mg/L
Mg^{2+}	1,310 mg/L	42,370 mg/L

Table 2. The content of metal cation in each lithium resources

Conditions	HMO	M-HMO		
	Adsorption	Adsorption	Desorption	Selectivity
pH	10.10±0.01	10.10±0.01	0.5 M HCl	10.10±0.01
Time	3 days	3 days	1 day	3 days
Temperature	298 K	298K	298K	298K
Li^+ concentration	10.0 mmol (~70 ppm)	10.0 mmol (~70 ppm)	0	10.0 mmol, Li^+ Na^+, K^+, Mg^{2+}

Table 3. Conditions for each adsorption tests

3. Results and discussion

3.1 Characterization

The synthesis procedure include two steps. First, spinel structure lithium manganese oxide (LMO) having different Li/Mn ratio and other properties were obtained by hydrothermal method. Then, on the surface of the prepared LMO, magnetite crystal phase was constructed by Fe^{2+} redox reaction in hydrothermal conditions where magnetite-LMO composites were obtained.

3.1.1 Characterization of LMO

The powder X-ray diffraction (XRD) analysis was conducted for the hydrothermally synthesized LMOs in order to identify crystal phase of LMO. As the representative sample, the XRD pattern of the nanocrystal lithium manganese oxide (LMO) synthesized using 2.0 M LiOH solution (LMO-2.0) and delithiated LMO after acid treatment (AT/LMO) are presented in Figure 11. In XRD pattern, LMO shows a cubic spinel crystal structure having all diffraction peaks corresponding to the (1 1 1), (3 1 1), (2 2 2), (4 0 0), (3 3 1), (5 1 1), (4 4 0), (5 3 1) which are similar with the spinel crystal XRD pattern of lithium manganese oxide in JCPDS 35-0782 (Joint Committee on Powder Diffraction Standards, No. 35-0782). For the acid-treated sample (AT/LMO), although the intensity of overall peaks become weaker, it maintains cubic spinel crystal structure even after acid treatment. In this result, it is noticeable that LMO and AT/LMO have quite similar XRD patterns with **8.25 and 8.03** Å lattice constants, respectively. Those lattice values demonstrate that the lattice crystal composed with Mn-O is quite

stable while Li^+ in lattice is extracted or exchanged during acid treatment. In addition, when little swelling and shrinking of lattice happen, the structure does not collapse and the location of each elements are well maintained. This phenomenon provide that the adsorbent from LMO is suitable material for recovery of lithium and repeated adsorption.

For the synthesized LMO from different concentration LiOH solutions (2.0 M, 2.5 M, 3.0 M), these XRD pattern are shown in Figure 12. All sample have similar XRD patterns having the diffraction peaks indicating spinel crystal structure appear. As LiOH amount increase, lattice parameter of cubic spinel structure decrease. Also, the relative peak intensity of (4 0 0)/(3 1 1) plane with increasing of LiOH amount increase. Table 4 presents the ratio value for the each samples. These phenomenon are caused by excess lithium ions brought on spinel structure of LMO. As I explained in introduction section, spinel structure in $LiMn_2O_4$ is organized with oxygen forming cubic closed-packed frame of crystal, manganese occupying half octahedron sites (16 d) and lithium occupying one-eighth tetrahedron sites (8a). Then, excess lithium ion brought into spinel structure become occupying the 16 d octahedron sites, which reduce the effect of the Jahn-Teller deformation [43]. Therefore, the decrease of lattice parameters with increasing of LiOH amount could be explained by increased lithium contents occupying octahedron sites. In addition, this possibly demonstrates the higher growth speed of (4 0 0) plane than that of (3 0 0) plane with increasing LiOH amount in lithium manganese oxide [7]. The chemical analysis result summarized in Table 4 provides supporting information for the explanations of the XRD results, which Li/Mn ratio in the synthesized samples increase with increasing of LiOH amount. Therefore, these results suggest that more lithium ion occupy in octahedron sites as introducing

more lithium ion in spine structure in present samples.

Using FWHM of three main diffraction peaks, (1 1 1), (3 1 1), (4 0 0) in XRD pattern of LMO, the average crystallite sizes for the each samples were calculated by adopting Debye-Scherrer equation:

[Debye-Scherrer equation]

$$D = K\lambda/\beta\cos\theta$$

(K = 0.89, λ = wavelength of radiation, β = FWHM, θ = Bragg angle (radian))

Specific surface area of each samples are measured with BET analysis method by adsorbing and desorbing nitrogen. The calculated average primary crystallite size and the measured surface area are summarized in Table 1. The decreasing tendency of crystallite size with increasing LiOH amount could be explained by the dependency of primary crystallite size on concentration of hydroxide ion [44]. As hydroxide ion concentration of solution increase, electrical repulsive force on the surface of LMO nanoparticle become greater, which suppress the further growth of LMO nanoparticle. This effect of hydroxide ion for preparation of LMO possibly demonstrate the increasing specific surface area as crystallite size of LMO decrease. The tendencies of crystallite size and BET specific surface area are well matched with each other.

Figure 13 shows the HR-TEM images of LMO. Since there is no remarkable differences between all samples, image of LMO-2.0 is shown as a representative example. As Figure 13 (a) shows, most LMO nanoparticles are agglomerated in cluster forms due to high surface energy from their small particle size. In TEM image, the particles show similar shape which is between rectangular and sphere. According to HR-TEM and FFT image on a particle of LMO in Figure 13 (b), distinct crystal planes appear on a particle and the distance between planes is 4.827 Å well agreed with the lattice d-spacing of the most dominant plane in XRD, (1 1 1) plane.

The results of the chemical analysis for each spinel structure LMOs are summarized in Table 1. As LiOH reagent amount increase, Li/Mn ratio and Z_{Mn} tend to increase. The average manganese oxidation numbers of LMO-2.5 and LMO-3.0 is approximate 4.00 in which Mn(IV) constitutes most manganese of LMO crystal compared with Mn(III) proportion in LMO. Therefore, the LMOs are expected to be chemically stable by composing LMO crystal with single and higher valence manganese. [45-46] Also both LMO crystal is possibly stable during acid treatment having less proportion of Mn(IV) which is the main component causing the dissolution of LMO crystal in the following lithium desertion process:

Ion exchange:

$$LiMn_2O_4 + H^+ \rightarrow HMn_2O_4 + Li^+$$

Redox reaction:

$$LiMn^{3+}Mn^{4+}O_4 + 2H^+ \rightarrow Li^+ + 0.5Mn^{2+} + H_2O + Mn^{4+}{}_{1.5}O_3$$

Lithium desertion process is carried out in acid solution with the two reactions, ion exchange reaction and redox reaction. Generally, it is known that redox reaction for lithium desertion is the main reason for the dissolution of LMO crystal and Mn(III) cause redox reaction while some portion of Mn(IV) is oxidized to Mn(IV) and other portion is reduced to Mn(II) as the above reaction. Therefore, the proportion of Mn(III) in LMO could provide the indication of chemical stability of LMO, which can be predicted with according to Li/Mn ratio and Z_{Mn} value of LMO [20]. Depending on this information, it is concluded that LMO-2.5 and 3.0 is predicted as the more stable LMO than LMO-1.0 and 2.0.

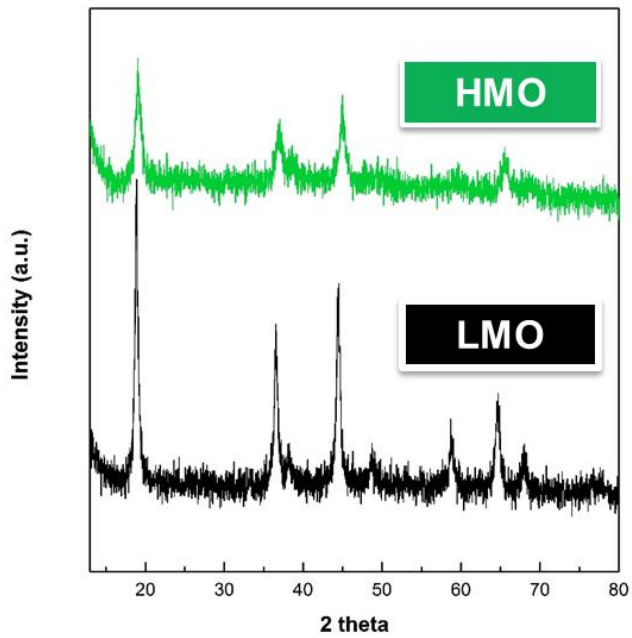

Figure 11. XRD patterns of the synthesized LMO and the acid treated LMO, HMO

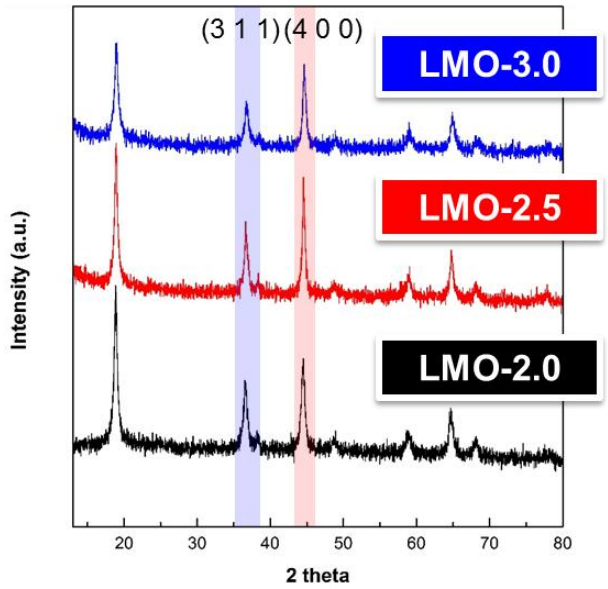

Figure 12. XRD patterns of LMOs synthesized from different amounts of lithium precursor, LiOH

Sample	(4 0 0)/(3 1 1) peak ratio	Li/Mn ratio	Z_{Mn} [Mn^{z+}]	Chemical formula	Average crystallite size*	BET surface area
LMO-2.0	1.10	~0.625	~3.89	$Li_{1.10}Mn_{1.77}O_4$	18.2 nm	93.95 m^2/g
LMO-2.5	1.29	~0.825	~4.00	$Li_{1.37}Mn_{1.66}O_4$	16.9 nm	113.11 m^2/g
LMO-3.0	1.33	~1.002	~4.00	$Li_{1.60}Mn_{1.60}O_4$	15.7 nm	150.92 m^2/g

Table 4. Summarized results of LMOs from each characterization

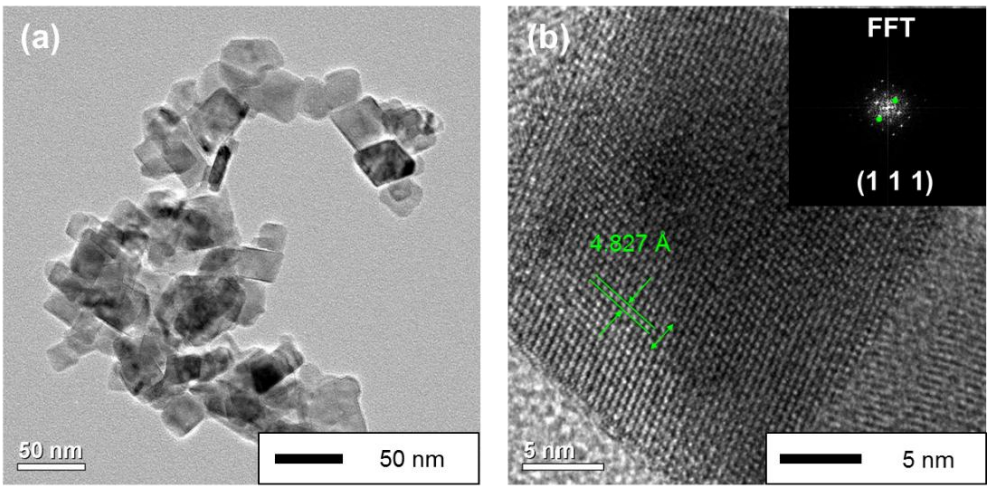

Figure 13. HR-TEM image of LMO; (a) agglomerated LMO cluster (b) HR image showing lattices spacing of (1 1 1) plane in LMO

3.1.2 Characterization of M-LMO

The synthetic routes for magnetite-lithium manganese oxide nanocomposite (M-LMO) begins with the synthesis of LMO. Using the synthesized LMO, magnetite-lithium manganese oxide were prepared by hydrothermally reacting the mixture of ferrous hydroxide ($Fe(OH)_2$) solution and LMO-dispersed solution. In order to synthesize the optimized synthetic conditions, several variations which possibly affect the products were selected and adjusted to the proper condition.

Figure 14. Show the XRD patterns of the representative M-LMO sample synthesized from LMO-2.0 sample, indicating the existence of two crystal phases in M-LMO sample. In the XRD pattern, most main diffraction peaks are allocated with specific diagrams, an inverted triangle (▼) and a circle (●) corresponding to each crystal phase: lithium manganese oxide (▼) and magnetite (●). Since the crystal structures of magnetite and LMO are similar with LMO having spinel structure and magnetite having inverse spinel structure respectively, it might be difficult to differentiate the XRD pattern into two definite crystal XRD pattern. However, each crystals have the dominant diffraction peak individually, which makes the each crystal phase looked more definitely. Therefore, two major diffraction peaks of (1 1 1) and (3 1 1) which are assigned to the dominant diffraction peaks for LMO and magnetite are conformed, which means the existence of two crystal phase in the synthesized M-LMO particles. Also, the asymmetric (3 1 1) diffraction peak indicate that there are more than two peaks overlapped in the range of 34-37.5°, corresponding to the 2theta value of (3 1 1) for LMO and magnetite.

The morphologies and crystallography of the synthesized M-LMO

were examined by HR-TEM. Figure 15 shows HR-TEM and FFT images of M-LMO. As seen in Figure 15(a), the typical particle nanostructure of M-LMO is an irregular agglomeration. Primary nanocrystals having uncertain shapes between sphere and rectangular constitute the irregular agglomeration. There is no distinctive change on the morphology compared with TEM images of LMO, which is attributed to the fabrication method for growing magnetite crystal phase on LMO surface. On the HR image of Figure15 (b), two kinds of crystal patterns can be found on a primary particle of M-LMO and those FFT images and marks on the images indicates they have different interplanar patterns. The interplanar spacing calculated from each FFTs are 0.486 nm and 0.270 nm approximate to d-spacing value of (1 1 1) and (3 1 1) from XRD, which are the dominant lattice planes in LMO and magnetite, respectively. Therefore, these results are well consistent with the XRD result of M-LMO.

While hybridizing the two materials with the method brought up in experimental section, some severe change on the crystal state of LMO was found from M-LMO. As seen by Figure 16 which compare XRD of M-LMO with the mixture of individually synthesized LMO and magnetite in 1:1 mass ratio, although the diffraction peaks in both XRD patterns were consistent on the similar 2theta position, entire feature of XRD pattern were different in two results. Therefore, it was proved that the product was not the mixture configuration. Then, to study the changes in the electronic state of manganese and iron ions on the surface of M-LMO, the synthesized M-LMO and LMO were examined by XPS measurement.

Figure 17 is the XPS results in the range of Mn 2p-assigned binding energy (635-665 eV). Mn $2P_{1/2}$ peak in the range of 654-658 eV disappear in M-LMO result, which might be caused by overlapping auger peak from

Fe auger electron with Mn $2P_{1/2}$ peak. With discerning the peaks of both M-LMO and LMO, it is found that there is a shift of XPS graph to lower binding energies from LMO to M-LMO in an entire Mn range. Mn $2P_{3/2}$ peak of LMO (643.5 eV) is shifted to lower binding energy (642.1 eV), which could be understood as the reduction of manganese oxidation state in each samples according to the other researches [47]. In order to find the meaning of the phenomenon for the reaction, literature search was carried out and it was found that there is the electron exchange reaction between Fe^{2+} and Mn^{3+} [48].

$$\mathbf{Fe^{2+} + Mn^{3+} \rightarrow Fe^{3+} + Mn^{2+} \qquad \Delta H = -6.2\ kcal}$$

Therefore, it was suggested that the reduction in oxidation state of Mn is possibly caused by the electron exchange between Fe^{2+} and Mn^{z+} of LMO in $Fe(OH)_2$ solution. As a related reaction of the interaction between LMO and Fe^{2+} in alkaline environment, the reaction of an oxidative ore, montmorillonite, in Fe^{2+} alkaline solution was found during literature search [49]. In the reported work, magnetite phase was easily formed with precipitation when montmorillonite was added into Fe^{2+} alkaline solution. On the basis of this result and literature searching, I could derive a mechanism which might explain the reaction process for the formation of magnetite phase on LMO. The following explanation is the proposed description for the reaction mechanism.

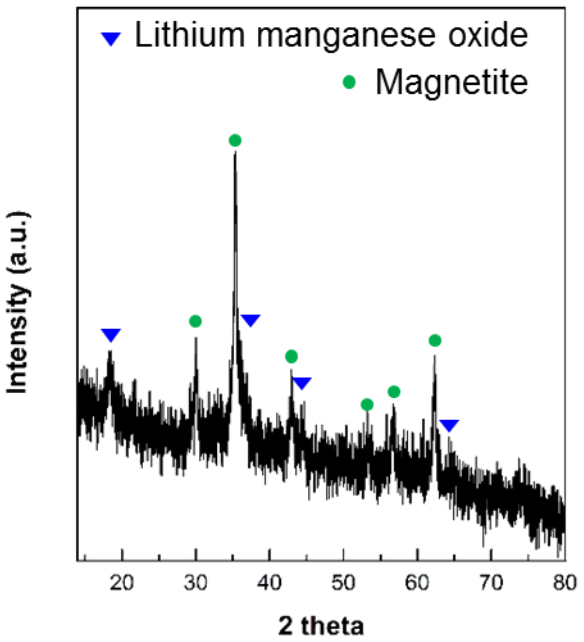

Figure 14. XRD pattern of the synthesized M-LMO, lithium manganese oxide (▼) and magnetite (●)

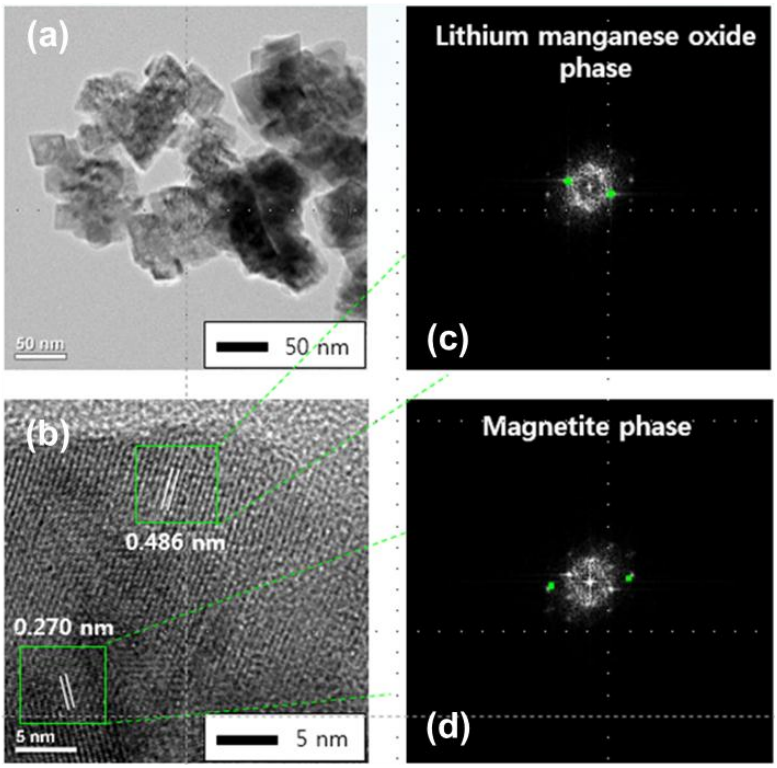

Figure 15. HR-TEM images of M-LMO; (a) TEM image of M-LMO nanoparticles, (b) HR image of a M-LMO particle showing two lattice planes, (c) FFT image in (b) corresponding to (1 1 1) of LMO, (d) FFT image in (b) corresponding to (3 1 1) of magnetite

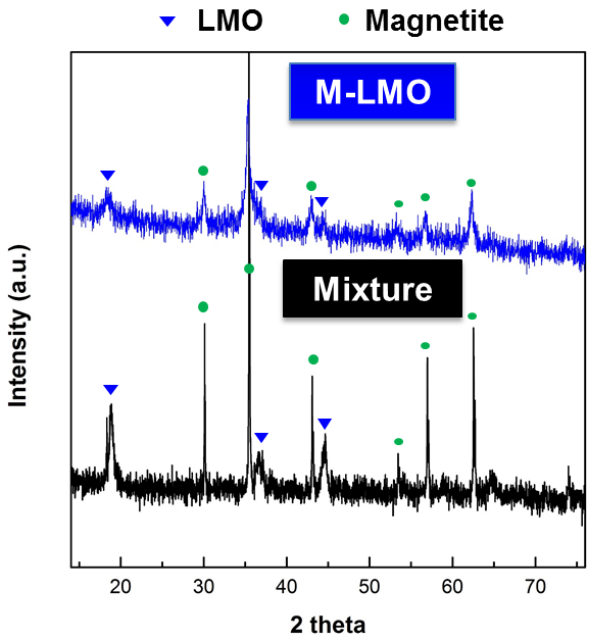

Figure 16. Comparison of XRD patterns of M-LMO and the mixture of LMO and magnetite (mass ratio 1:1)

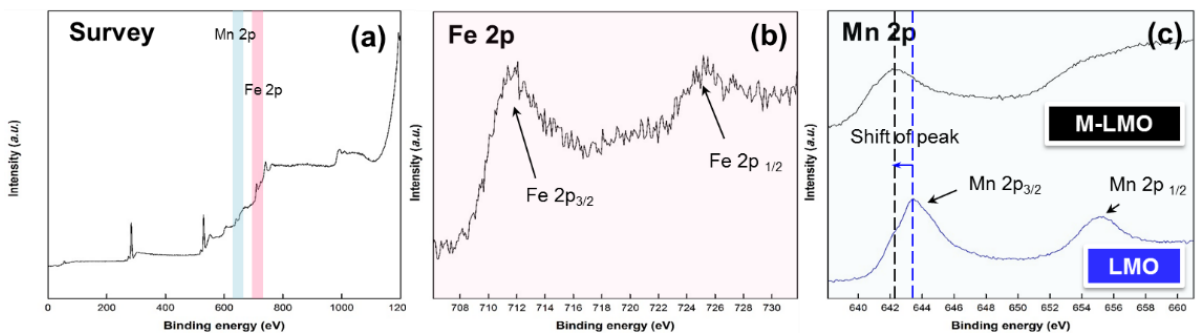

Figure 17. XPS spectra of M-LMO; (a) survey spectrum of M-LMO, (b) M-LMO spectra in Fe 2p region, (c) M-LMO spectra in Mn 2p region where peak shift from Mn 2p of LMO occurs

When LMO solution is added into $Fe(OH)_2$ solution in N_2 atmosphere, manganese ion on the surface of LMO react with Fe^{2+} ion in $Fe(OH)_2$ solution while exchanging electrons between each other. Then, Fe^{2+} become oxidized to Fe^{3+} and at the same time, manganese ion having 3.5-4.0 of oxidation states on LMO is reduced to lower oxidation states.

$$Mn^{Z+} + Fe^{2+} + nOH^- \rightarrow Mn^{A+} + Fe^{3+} + nOH^- \rightarrow Mn^{A+} + Fe(OH)_3$$

(**Z: 3.5-4.0**, **A: <3.5**)

As a result of the oxidation of Fe^{2+}, the $Fe(OH)_3$ precipitation is formed on the LMO surface, which is converted into magnetite phase by co-precipitation reaction with $Fe(OH)_2$ in the mixed solution. The similar reaction of $Fe(OH)_2$ occurs with minerals having oxidizing property [49].

Co-precipitation reaction

$$Fe^{2+} + 2Fe^{3+} + 8OH^- \rightarrow Fe_3O_4 + H_2O$$

Schikorr reaction

$$3Fe(OH)_2 \rightarrow Fe_3O_4 + 2H_2O + H_2 \quad (> 373K)$$

Then, the unreacted $Fe(OH)_2$ is decomposed in high temperature (>373 K) while producing magnetite, water and hydrogen according to Schikorr reaction [50].

The magnetite phase from Schikorr reaction is dissolved and redeposit onto the already formed magnetite phase on LMO surface with Ostwald ripening process. In the end of these reactions, magnetite crystal phase become built up on the surface of LMO and magnetite-lithium manganese oxide nanocomposite (M-LMO) is produced. As shown by the above description, when manganese on LMO become reduced by Fe^{2+} in $Fe(OH)_2$ solution, the reduction of manganese possibly cause the destruction of LMO crystal phase by changing the arrange of manganese in the LMO lattice. Therefore, on the basis of the proposed mechanism, the controlled preparation of M-LMO with several variations were carried in order to find the preparation condition for minimizing the destruction of LMO crystal and maximizing magnetization of M-LMO. The destruction of LMO during reaction is controlled by adjusting the dispersity of the LMO-dispersed solution and the condition of Schikorr reaction with additives, and the experiments for adjusting a condition for the growth of magnetite are carried out for maximizing magnetization of M-LMO.

The experiments for controlling LMO destruction degree were carried out by adjusting the dispersity of LMOs in solution mixture and the condition of Schikorr reaction. The solvent amount of the mixture solution of LMO and $Fe(OH)_2$ is presumed to adjust the dispersity of LMO during the fabrication. According to the previous studies, colloid volume fraction influences the degree of dispersion as having more compact cluster in two

and three dimensions at higher colloidal density. [51-52] Thus, the preparation of M-LMO was performed with the variation of volume of $Fe(OH)_2$ solution with 30, 60, 90 mL. Other conditions are fixed by using LMO-2.0 as the LMO precursor, 4.5 mL $NaOH_{aq}$ (40%) and same amount other reagents. As solution volume increase, when the LMO solution is added into the $Fe(OH)_2$ solution, the dispersity of the mixture solution is presumed to increase. Table 5 shows the Li and Mn molar ratio (Li/Mn) of M-LMO which are from compositional analysis result. The value of Li/Mn ratio for all M-LMO are lower than that of LMO having approximate 0.625. This decrease in Li/Mn ratio possibly explain the destruction phenomenon of LMO crystal during the fabrication of M-LMO, which are described in the proposed mechanism. According to the result, Li/Mn ratio tends to decrease as solvent amount become increased. This tendency could indicate that the increase in dispersity of LMO in mixture with increasing of solvent amount leads to enlarge the reacted surface area of LMO with Fe^{2+} by reducing Mn ion ion LMO, which cause to increase in the portion of losing LMO phase according to the proposed mechanism.

Furthermore, the condition of Schikorr reaction was varied by changing additives to control the destruction of LMO. According to the reported work [53], the existence of complex agents in $Fe(OH)_2$ solution could affect Schikorr reaction conditions. In this work, it is proved that Schikorr reaction is inhibited when the stability of $Fe(OH)_2$ become higher as the complexation of $Fe(OH)_2$ is formed. The work explain that the stability of complex is depending on the functional groups in complex agent which can adsorb or complex with metal ion. Therefore, in my work, sodium acetate (CH_3COONa) and glutamic acid ($C_5H_9NO_4$) were used during the preparation of M-LMO in order to confirm the effects of the complex

strength with Fe^{2+} on the synthesized M-LMO and the destruction of LMO in M-LMO. As seen by chemical structure of each additives in Figure 20, glutamic acid (glutamate) has two carboxyl groups and one amine group which have strong affinity to metal cation and it could have higher complex strength than sodium acetate. As a result of compositional analysis of M-LMO from each additives in Table 6, M-LMO from glutamic acid have lower Li/Mn ratio than M-LMO from sodium acetate, which means that more destruction LMO proceeds in M-LMO from glutamic acid. On a basis of the reported work, it is probably explained that as glutamic acid is used for additive, the inhibited Schikorr reaction keeps Fe^{2+} from turning into Fe_3O_4. Instead, the remained Fe^{2+} reacts with manganese in LMO phase additionally, which causes the additional destruction of LMO phase.

The control of magnetization of M-LMO was performed by the experiment for adjusting magnetite phase. Several research groups [54-55] reported that magnetite crystal phase could be controlled by varying the content of reagents which could adjust surface charge, such as alkaline sources. The experiments for controlling magnetite phase formed on LMO were carried out by adjusting 40 % NaOH solution amounts in M-LMO preparation method: 3.0, 4.5, 6.0 mL. Applying Debye-Scherrer equation and (3 1 1)'s FWHM derived from XRD result of M-LMOs in Figure 21, the crystallite sizes of (3 1 1) lattice plane which are the most dominant diffraction peak of magnetite crystal phase are calculated for each M-LMOs. The calculated results in Table 7 indicates that the crystallite of magnetite is likely to decrease as hydroxide ion or negative charge in solution increase. This is possibly because magnetite particle surface become charged with hydroxide ion, which could restrict the growth of magnetite particle with enhancing electrostatic repulsion as the description of Figure 23 illustrates.

In the VSM result of Figure 22, the saturation magnetization of M-LMO decreases with increasing of hydroxide ion amount, which are consistent of the results of the calculated (3 1 1) crystallite size for each samples because the magnetite crystal size and the surface proportion to the crystal affect the magnetization involving surface disorder at the particle surface [56]. Besides, in the XRD pattern of M-LMO from 6.0 mL 40% $NaOH_{aq}$, the additional peak at 33.27 ° appears and this peak might be involved with the (1 0 4) diffraction peak of hematite according to JCPDS 33-0664. Therefore, the addition of 3.0 mL 40 % $NaOH_{aq}$ for preparation of M-LMO is seemed to be a proper quantity for the nanocomposite separable from liquid medium due to relatively higher magnetization. This was verified by separating the M-LMO particle from water medium with approaching of magnet to the water medium like the pictures of Figure 24.

With the optimized preparation recipe, 30 mL solvent volume, sodium acetate as an additive and 3.0 mL 40 % $NaOH_{aq}$, from the earlier experiments, M-LMOs for each LMO samples, LMO-2.0, 2.5, 3.0, were prepared. The M-LMO samples are named depending on the LMO precursors, as M-LMO-2.0, 2.5, 3.0. There is no distinctive difference for M-LMOs from each LMO in XRD pattern of Figure 25. In VSM result of Figure 26, for measuring magnetizations, each M-LMO have different magnetic properties depending on LMO precursors. As the precursor of M-LMO changes from LMO-2.0 to LMO-3.0, the saturation magnetization (M_s) of M-LMOs tend to decline from 44.42 emu/g to 25.02 emu/g. This tendency might be caused by the difference on the size of precursors, LMO. LMO precursor could play a role of the foundation where magnetite phase is built for establishing composite. Therefore, the size of magnetite crystal is possibly affected by the crystal size of LMO. As seen by Table 8, the

calculated crystallite size of (3 1 1) of M-LMO, the representative diffraction peak of magnetite, decrease with changing LMO from 2.0 to 3.0 which are well agreed with the calculated crystallite size of LMOs in Table 4. Therefore, the particle size reduction and the increment of surface ratio to intact crystal of magnetite lead to the reduction of magnetization for each M-LMOs. This explanation is more feasible because the mass ratio of magnetite in the composite are quite similar with all M-LMOs as shown in Table 8, which means that the compositional difference for each M-LMOs do not largely affects the magnetization of M-LMO. This mass ratio is calculated using Li/Mn ratio and Fe/Mn ratio from compositional analysis and chemical formula of LMO under the hypothesis that all manganese component in M-LMO come from LMO and iron (ferrous or ferric) component from magnetite, Fe_3O_4. According to this result of Table 8, the magnetite portion in M-LMO tends to increase with changing LMO precursor from 2.0 to 3.0. This might be from the effect of LMO's surface area where Fe^{2+} of $Fe(OH)_2$ react with manganese of LMO. Using these M-LMOs, M-LMO-2.0, 2.5, 3.0, and the LMO precursors, LMO-2.0, 2.5, 3.0, the lithium adsorption tests were carried out after immersing the samples in HCl solution for 24 h.

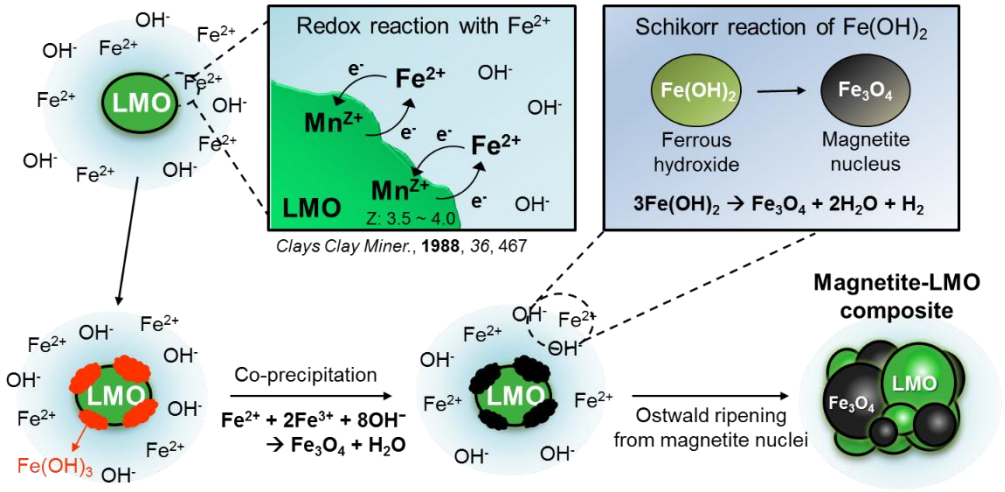

Figure 18. Schematic diagram of the proposed mechanism for the hybridizing reaction

Variation	Li/Mn ratio
30 mL	0.196
60 mL	0.161
90 mL	0.147

Table 5. Li/Mn molar ratio of M-LMO synthesized in different solvent volumes

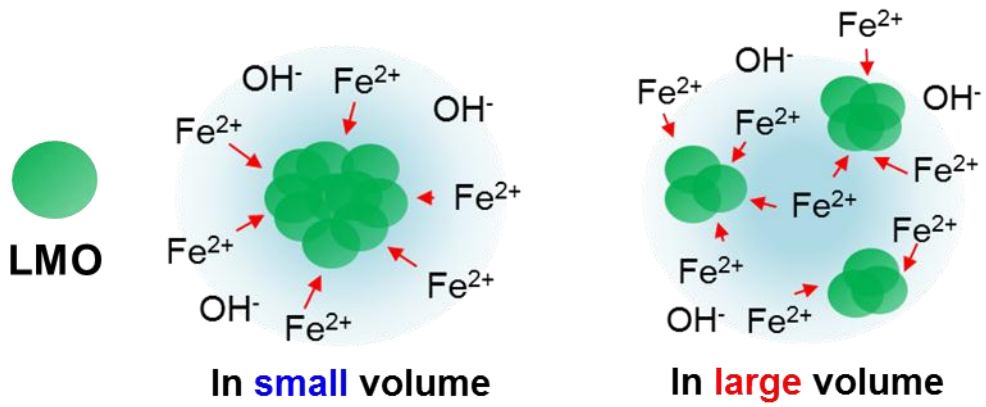

Figure 19. Descriptions for the adjustment of dispersity of LMO with varying solvent volume

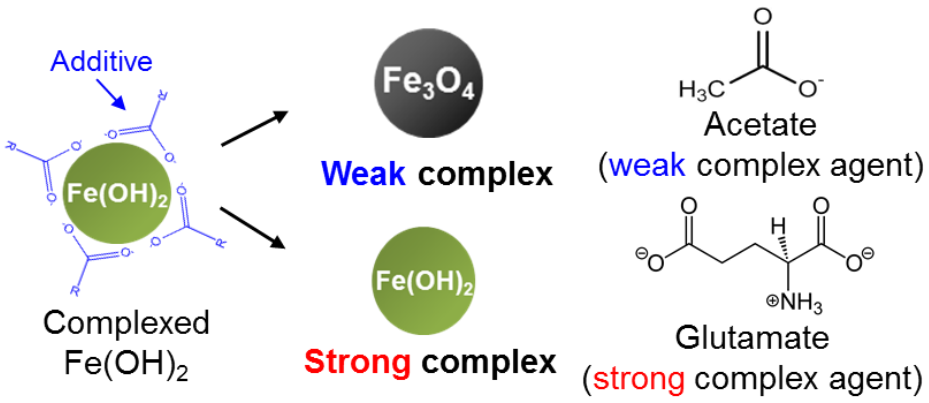

Figure 20. Description illustrating the tendency for Schikorr reaction depending on the complex agents, acetate and glutamate

Variation	Li/Mn ratio
Acetate	0.196
Glutamate	0.075

Table 6. Li/Mn molar ratio of M-LMOs synthesized in different complex agents

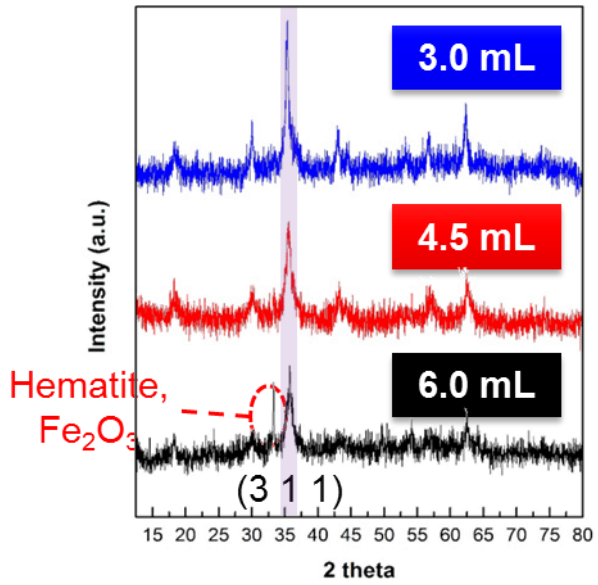

Figure 21. XRD patterns for M-LMOs synthesized by different 40% $NaOH_{aq}$ amounts

Variation	Crystallite size of (3 1 1)	Saturation magnetization (M_s)
3.0 mL	26.2 nm	44.42 emu/g
4.5 mL	13.1 nm	26.57 emu/g
6.0 mL	10.5 nm	25.30 emu/g

Table 7. Crystallite size of (3 1 1) lattice plane calculated from XRD information and Saturation magnetization (M_s) of M-LMOs synthesized by different 40% $NaOH_{aq}$ amounts

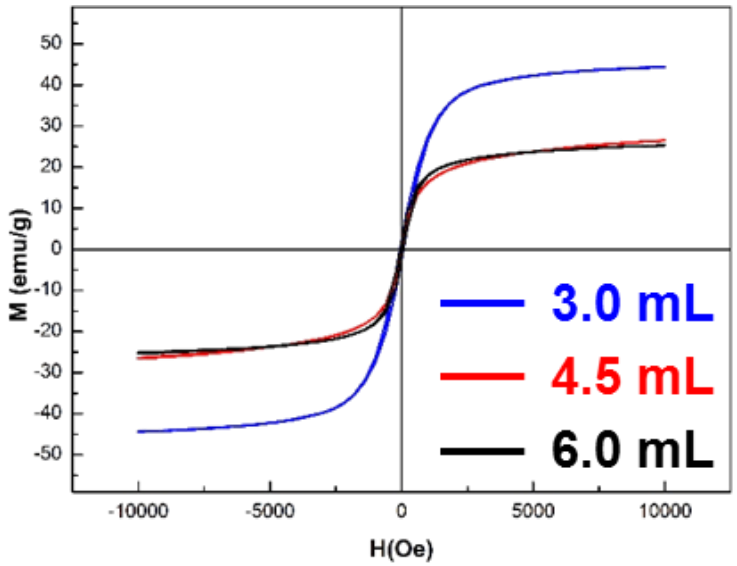

Figure 22. VSM results of M-LMOs synthesized by different 40% $NaOH_{aq}$ amounts

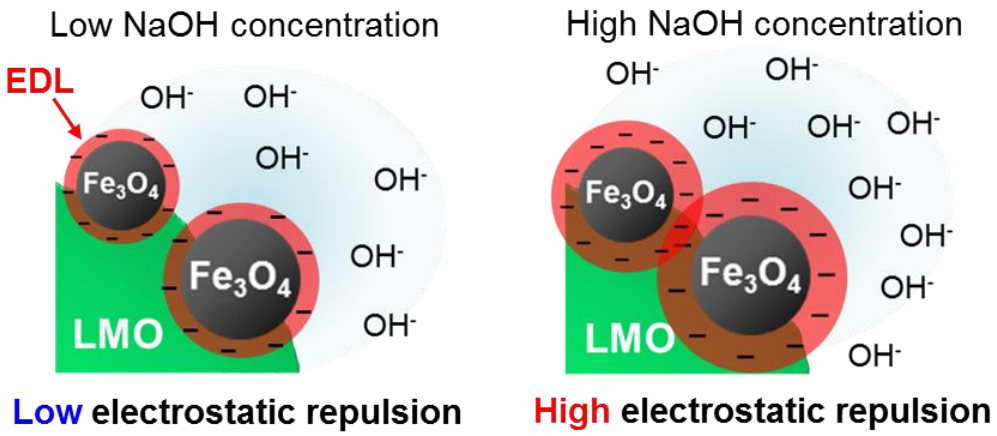

Figure 23. The description illustrating the effect of hydroxide ion amount on the growth of Fe_3O_4 phase

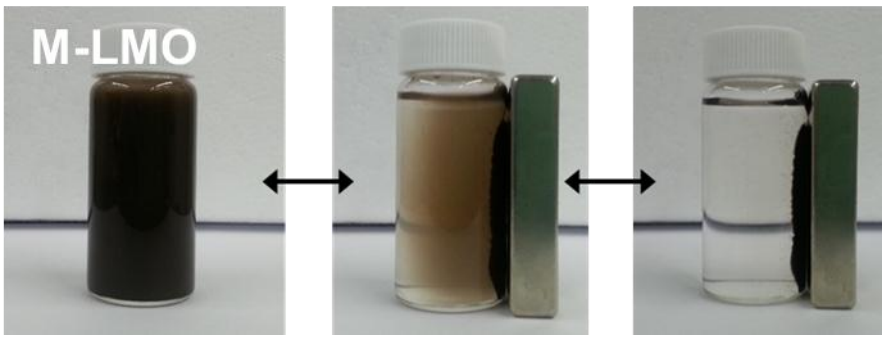

Figure 24. Separation of magnetic M-LMO from water with magnet

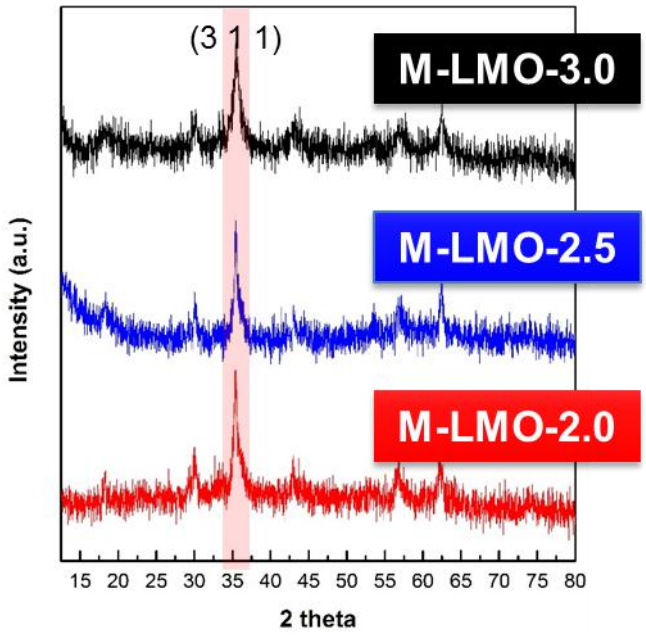

Figure 25. XRD patterns for M-LMOs synthesized from different LMO precursor

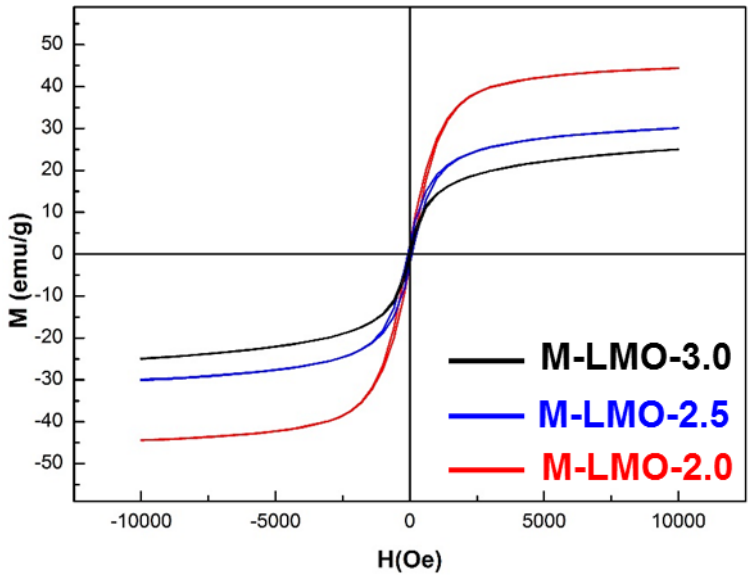

Figure 26. VSM result of M-LMOs synthesized from different LMO precursor

Variation	Li/Mn ratio	Fe/Mn ratio	BET surface area	Crystallite size of (3 1 1)	Saturation magnetization (M_s)	Mass ratio (LMO : magnetite)
M-LMO-2.0	0.196	1.308	357.0 m^2/g	26.2 nm	44.42 emu/g	**0.945 : 1.000**
M-LMO-2.5	0.214	1.377	401.7 m^2/g	17.5 nm	30.09 emu/g	**0.934 : 1.000**
M-LMO-3.0	0.330	1.421	409.9 m^2/g	15.0 nm	25.02 emu/g	**0.929 : 1.000**

Table 8. Summarized results table of M-LMOs from several characterizations

3.2 Evaluation of lithium adsorptive properties

3.2.1. Equilibrium lithium ion adsorption test for LMOs and M-LMOs

Lithium adsorption test were performed in 10 mmol/L Li^+ (69.4 mg/L Li^+) concentration solution having pH 10.10 at 298 K. The lithium adsorption capacity were examined by the Li^+ extracted samples (HMOs and M-HMOs) after acid treatment of LMO-2.0, 2.5, 3.0 and M-LMO-2.0, 2.5, 3.0. Figure 27 shows the adsorption result of each HMOs displaying the relation between lithium adsorption capacity and Li/Mn ratio of the LMO precursors. The result shows that the capacity for lithium increase with the increase of Li/Mn ratio contained in LMO crystal. From this result, it is suggested that lithium adsorptive sites in spinel structure could be developed from lithium sites arranged in spinel LMO crystal. Besides, surface area of LMO precursor could be a factor to increase lithium adsorption capacity of HMOs. With this LMO having 20.84-30.61 mg/g capacity, M-LMOs were prepared and tested for measuring their lithium adsorption capacity.

In order to compare the maximum capacity of HMO in M-HMO with the experimentally obtained capacity of M-HMO, I designed an equation for estimating the maximum capacity (mg/g) of HMO in M-HMO composite. The maximum capacity of HMO in M-HMO is calculated by multiplying the lithium capacity of HMOs from each LMOs and the mass ratio of LMO in M-LMO composite which was calculated.

$$\begin{array}{c}\text{HMO's}\\ \text{capacity for Li}\\ \text{(unit: mg/g)}\end{array} \times \begin{array}{c}\text{Mass ratio}\\ \text{of LMO}\\ \text{in composite}\end{array} = \begin{array}{c}\text{Calculated}\\ \text{capacity of HMO}\\ \text{in composite}\\ \text{(unit: mg/g)}\end{array}$$

As a result, Figure 28 shows the columns chart comparing the calculated maximum capacity and the experimentally obtained capacity of M-HMOs. And in Table 9, there is a percent ratio of the experimental capacity to the calculated maximum capacity for each M-HMOs. According to these ratio values, M-HMOs from LMO-2.5, 3.0 show better lithium adsorption performance close to the calculated capacity by having 58.31 % and 50.00 % of original LMO's capacity. This result suggests that the prepared M-LMO from the chemically more stable LMO can maintain its LMO's lithium adsorption capacity better. LMO-2.5 and 3.0 have singular and higher oxidation state of manganese than that of LMO-2.0 by having 4.00 oxidation number. Generally, it is known that metal oxides having singular and high valence form of metal are chemically stable due to strengthen Me-O bonds to the lattice [45]. And the lower value of M-HMO-3.0 might be caused by the higher surface area of LMO-3.0 resulting in the further destruction of LMO. These lithium-adsorbed M-HMOs were treated with acid solution again for reusing in other lithium adsorption test.

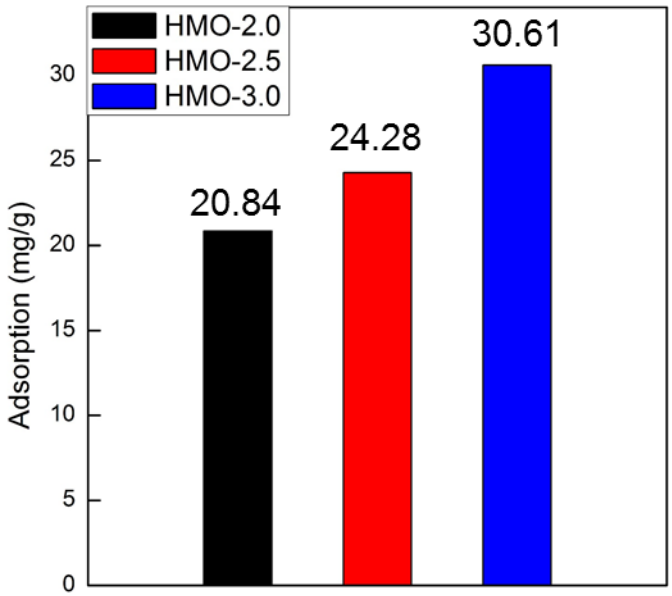

Figure 27. Adsorption capacity of each HMOs

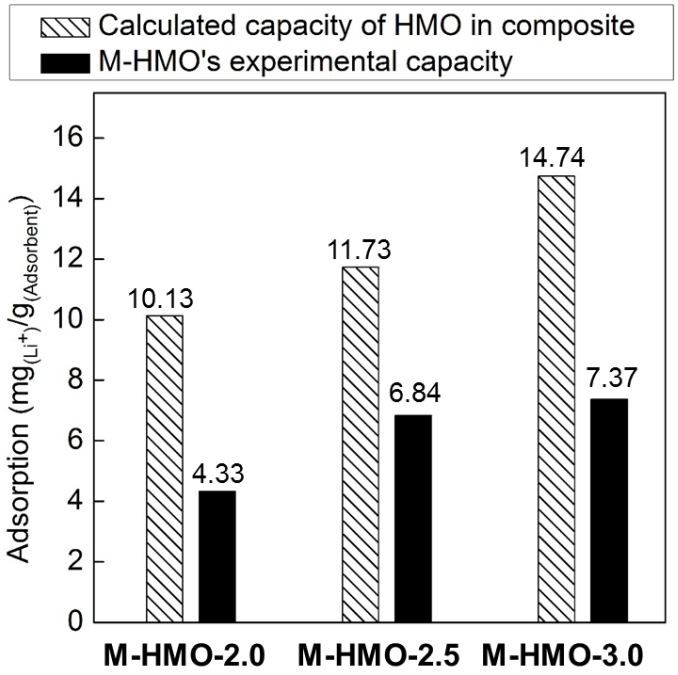

Figure 28. Adsorption capacity of M-HMOs and comparison with calculated capacity of maximum capacity of M-HMO

Composite	Mass ratio of LMO	Experimental /Calculated capacity
M-HMO-2.0	0.486	42.74 %
M-HMO-2.5	0.483	58.31 %
M-HMO-3.0	0.482	50.00 %

Table 9 Mass ratio of each M-LMOs and a percent ratio of the experimental capacity to the calculated one of M-HMOs

3.2.2 Repetitive lithium ion adsorption test of M-HMO

After a lithium adsorption test, the lithium-adsorbed M-HMOs were treated with acid solution to release adsorbed lithium ion and recover its lithium adsorptive properties. Then, the lithium adsorption tests were carried out again with these recovered M-HMOs. After that, these process was repeated. The adsorption results for each M-HMOs are presented in Figure 29. Totally, lithium adsorption tests were carried out three times. The performance of M-HMO-2.0 and 2.5 are maintained at roughly 90% of the initial adsorption capacity through the 3 times lithium adsorption tests. Therefore, this result suggested that those samples are appropriate for the repetitive lithium recovery system. However, the adsorption capacity of M-HMO-3.0 is remarkably declined for each tests compared with the initial capacity. Overall, the adsorption capacity of every M-HMOs tends to decrease during the repetitive test, which might be attributed by the acid treatment carried out before the lithium adsorption test. The instability of M-HMO-3.0 for the acid treatments might be caused by the small crystal size of LMO and magnetite. On a basis of the stability of the performance and the adsorption capacity, M-HMO-2.5 is determined as the most appropriate magnetite-lithium manganese oxide nanocomposite maintaining its initial performance at roughly 90% as shown in Table 10. In order to verify the feasibility for aqueous lithium resources, the selectivity test and lithium adsorption test in concentrated seawater were carried out using the M-HMO-2.5.

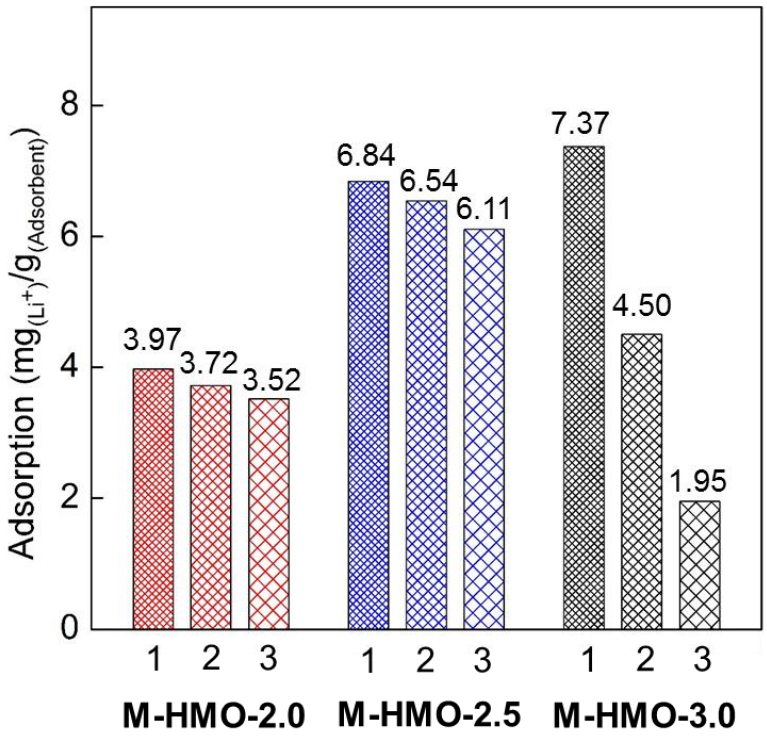

Figure 29. Result of repetitive adsorption tests of M-HMOs for three times

Sample	Recovery efficiency, R(%)※		
	1st	2nd	3rd
M-HMO-2.0	100.0	93.7	88.7
M-HMO-2.5	100.0	95.6	89.3
M-HMO-3.0	100.0	61.1	26.5

❖ R(%): recovery efficiency = $Q_r/Q_i \times 100$, where Q_i is the initial amount of adsorbed lithium, and Q_r is the amount of adsorbed lithium for reused adsorbent.

Table 10. Calculated recovery efficiency of M-HMOs

3.2.3 Selectivity for lithium ion and other cation of M-HMO

The adsorption selectivity for lithium ion was measured by estimating the distribution coefficient (K_d) for Li^+ and several cation, Na^+, K^+, Mg^{2+} which are the main elements co-existing in seawater, and comparing the value of Li^+ with others. The obtained results are shown in Figure 30. The Figure 30 indicates that the distribution coefficient (K_d) for Li^+ of M-HMO is high enough to be adsorbed selectively with excluding other cation. The K_d value of M-HMO for the metal cation are in the same order of Li^+ >> Mn^{2+} > Na^+ > K^+ with that of HMO. From this result, it is suggested that HMO crystal included in M-HMO is preserved and have its own property for selectively adsorbing Li^+ ion. Therefore, M-HMO could be an appropriate material to adsorb lithium ion selectively in the lithium aqueous resources where other cation coexist massively comparing with Li^+, such as brine, seawater and concentrated seawater.

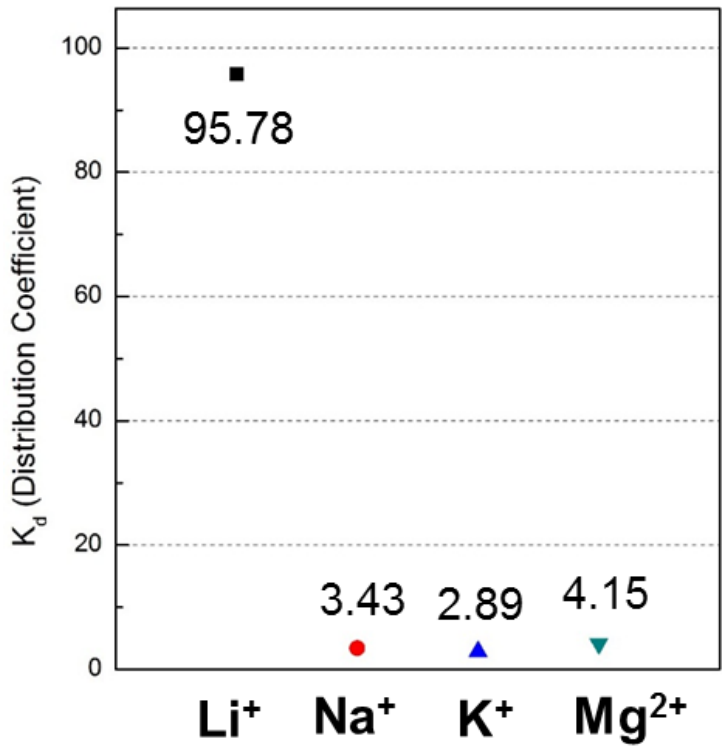

Figure 30. Distribution coefficient for each metal cation, Li^+, Na^+, K^+, and Mg^{2+}

3.2.4 Lithium adsorption test in concentrated seawater using M-HMO

Concentrated seawater is highly concentrated salt water with the evaporative process. Therefore, its concentration for each cation is enormously higher than regular seawater. Generally, in seawater, there are 10,900 mg/L Na^+, 1,310 Mg^{2+}, 390 K^+. The concentrated seawater have higher concentration of cation, 71,748 mg/L Na^+, 42,367 mg/L Mg^{2+}, 8,754 mg/L K^+ as seen by Table 2. However, the evaporative process also makes lithium ion concentrated like other cation. Although lithium ion in seawater exist in very low concentration, 0.15-0.20 mg/L which is not proper for industrial application, since the concentrated seawater have higher lithium ion, roughly 0.8 mg/L, lithium recovery from the concentrated seawater is expected to be effective and economically efficient. Compared with the lithium solution used in the previous adsorption tests, total lithium amount existing in the concentration seawater is too small to estimate the lithium adsorbing capability of M-HMO. Therefore, the adsorption test was carried out at 0.1 g/L adsorbent concentration. In the result, M-HMO show lithium adsorption properties having 1.02 mg/g lithium adsorption even in highly salty environment. This might be caused by the small concentration and the massive existence of other cation in the concentrated seawater reducing the chance for lithium ion to encounter the active site of M-HMO and adsorption rate.

4. Conclusion

In the present study, magnetite-lithium manganese oxide nanocomposite was prepared to realize magnetically water-separable and selectively lithium adsorbable material, and have been investigated by several analyses and performing various lithium adsorption tests. As a foundation where magnetite phase grows, lithium manganese oxide (LMO) synthesized from hydrothermal reaction was varied with lithium content in the spinel structure and analyzed for each LMOs. As lithium content increase, the oxidation number of manganese increase in LMO and the crystallite of LMO become smaller, which lead the increment of surface area, as well as Li/Mn atomic ratio of LMO increase from 0.625 to 1.002. Then, with varying lithium contents, LMOs having different properties were prepared for a precursor of composite and the chemical formula of each LMOs were calculated. To synthesize magnetite-lithium manganese oxide nanocomposite (M-LMO), LMO and $Fe(OH)_2$ mixture was treated with hydrothermal reaction, and the product was analyzed with XRD, HR-TEM and XPS. The results show that two crystal phase, magnetite and LMO were observed in the product, and with a magnet, it is conformed for the product to be magnetically separable from water. In addition, manganese oxidation state became reduced from the state of LMO after undergoing the reaction. After literature searching, the related reactions, found in other works, demonstrated that the phenomenon could be caused by Fe^{2+} redox reaction with Mn^{z+} in LMO, which might lead to the formation of magnetite. On a basis of the results and the literatures, I could devise a mechanism with which the product, magnetite-lithium manganese oxide could be formed. On the proposed mechanism, manganese in the added LMO exchanges electron with Fe^{2+} in $Fe(OH)_2$ solution, which cause to form $Fe(OH)_3$ which turn into magnetite phase with co-precipitation reaction. The

remained $Fe(OH)_2$ also turn into magnetite nuclei by Schikorr reaction, which become dissolved and redeposit on the magnetite phase on LMO with Ostwald ripening. In the end of these process, magnetite-lithium manganese oxide nanocomposite was prepared. And it was found that there could be LMO destruction while manganese become reduced by reacting Fe^{2+} in $Fe(OH)_2$ solution. On a basis of the proposed mechanism, the kind of additives, solvent amount, and OH^- amount were controlled to minimize LMO destruction occurred during the reaction and maximize magnetism of M-LMO. According to the results, the optimized preparation method was developed and used to synthesize M-LMOs from LMO-2.0, 2.5, 3.0. After treating these M-LMOs and the LMOs in acid solution, lithium adsorption tests were carried out and then, HMO showed 20.84-30.61 mg/g lithium adsorbing performance. M-HMOs from the LMOs also showed the lithium adsorbing properties even after the reaction for constructing composite. Then, among these M-HMOs, M-HMO-2.5 was determined as the most appropriate composite due to its better capacity, 6.84 mg/g, and stability of the composite structure for reusing than others. The M-HMO-2.5 was verified for its applicability for using in actual lithium aqueous resources by measuring the distribution coefficient (K_d) of cation including lithium having $Li^+ >> Mn^{2+} > Na^+ > K^+$ and conforming its lithium adsorbing properties in concentrated seawater. Therefore, these results demonstrate that magnetite-lithium manganese oxide nanocomposite (M-LMO) is a promising lithium adsorbent having a good potential in industrial lithium recovery system in aqueous lithium resources.

5. References

[1] U.S. Department of Energy, Critical Material Strategy, **2011**.

[2] P. W. Gruber, P. A. Medina, G. A. Keoleian, S. E. Kesler, M. P. Everson, T. J. Wallington, *J. Ind. Ecol.* **2011**, 15, 760-775.

[3] U.S. Geological Survey, Mineral Commodity Summaries, **2012**.

[4] S. E. Kesler, P. W. Gruber, P. A. Medina, G. A. Keoleian, *Ore Geology Reviews*, **2012**, *48*, 55–69

[5] R. Chitrakar, H. Kanoh, Y. Miyai, K. Ooi, *Ind. Eng. Chem. Res.* **2001**, *40*, 2054-2058.

[6] Q.-H. Zhang, S. Sun, S. Li, H. Jiang, J.-G. Yu, *Chem. Eng. Sci.* **2007**, *62*, 4869-4874.

[7] L. Wang, W. Ma, R. Liu, H. Y. Li, C. G. Meng, *Solid State Ionics.* **2006**, *177*, 1421-1428.

[8] Q.-H. Zhang, S.-P. Li, S.-Y. Sun, X.-S. Yin, J.-G. Yu, *Chem. Eng. Sci.* **2010,** *65*, 169-173

[9] L. Tian, W. Ma, M. Han, *Chem. Eng. J.* **2010,** *156*, 134-140.

[10] J.-L. Xiao, S.-Y. Sun, J. Wang, P. Li, J.-G. Yu, *Ind. Eng. Chem. Res.* **2013**, *52*, 11967 – 11973

[11] Z. Zhou, W. Qin, Y. Liu, W. Fei , *J. Chem. Eng. Data* **2012**, *57*, 82-86.

[12] Y. Nakatani, R. Ibrahim, S. Ogawa, *J. Am. Chem. Soc.* **2002**, *124*, 4936-4937.

[13] Z. Zhou, W. Qin, Y. Liu, W. Fei , *J. Chem. Eng. Data* **2012**, *57*, 82-86.

[14] S.-Y. Sun, X. Song, Q.-H. Zhang, J. Wang, J.-G. Yu, *Adsorption* **2011**, *17*, 881-887.

[15] T. Oi, M. Endoh, M. Narimoto, M. Hosoe, *J. Mater. Sci.* **2000**, *35*, 509-513.

[16] Q.-H. Zhang, S.-PengLi, S.-Y. Sun, X.-S.Yin, J.-G.Yu, *Chem. Eng. Sci.* **2010**, *65*, 165-168

[17] T. Oi, Y. Uchiyama, M. Hosoe, K. Itoh, *J. Nucl. Sci. Technol.* **1999,** *36*, 1064-1068

[18] M. H. Rossouw, A. de Kock, L. A. de Picciotto, M. M. Thackeray, *Mater. Res. Bull.* **1990**, *25*, 173-182.

[19] J. C. Hunter, *J. Solid State Chem.* **1981**, *39*, 142-147.

[20] Q. Feng, Y. Miyai, H. Kanoh, K. Ooi, *Langmuir* **1992**, *8*, 1861-1867.

[21] R. Chitrakar, H.Kanoh, Y. Miyai, K. Ooi, *Chem. Mater.* **2000**, *12*, 3151 - 3157.

[22] M. M. Thackeray, W. I. F. David, P. G. Bruce, J. B. Goodenough, *Mater. Res. Bull.* **1983**, *18*, 461-472.

[23] M. M. Thackeray, P. J. Johnson, L. A. de Piciotto, P. G. Bruce, J. B. Goodenough. Mater. Res. Bull. 1984, 19, 179-187.

[24] C. Ö zgür, *Solid State Ionics* **2010,** *181*, 1425–1428

[25] L. Wang, C. G. Meng, M. Han, W. Ma, *J. Collid. Interf. Sci*, **2008**, *325*, 31–40.

[26] J. Park, H. Sato, S. Nishihama, K. Yoshizuka, *Solvent Extr. Ion Exch.* **2012**, *30*, 398-404.

[27] R. Chitrakar, Y. Makita, K. Ooi , A. Sonoda, *Chem. Lett.* **2012**, *41*, 1647-1649.

[28] G. Xiao, K. Tong, L. Zhou, J. Xiao, S. Sun, P. Li, J. Yu, *Ind. Eng. Chem. Res.* **2012**, *51*, 10921-10929.

[29] R. Chitrakar, H. Kanoh, Y. Miyai, K. Ooi, *Chem. Mater.* **2000**, *12*, 3151-3157.

[30] Y. Onodera, T. Iwasaki, H. Hayashi, K. Torii, *Chem. Lett.* **1990**, *19*, 1801-1804.

[31] Y. Miyai, K. Ooi, T. Nishimura, J. Kumamoto, *Bull. Soc. Seawater Sci. Jpn.* **1994**, *48*, 411.

[32] Y. Han, H. Kim, J. Park, *Chem. Eng. J.* **2012**, *210*, 482–489.

[33] L.-W. Ma, B.-Z. Chen, Y. Chen, X.-C. Shi, *Micropor. Mesopor. Mat.* **2011**, *142*, 147

[34] A. Umeno, Y. Miyai, N. Takagi, R. Chitrakar, K. Sakane, K. Ooi, *Ind. Eng. Chem. Res.* **2002**, *41*, 4281-4287.

[35] Z. Ji, J. Yuan, X. Guo, J. Wang, L. Li, *Applied Mechanics and Materials,* **2012**, *161*, 144-147

[36] K.S. Chung, J.C. Lee, W.K. Kim, S.B. Kim, K.Y. Cho, *J. Membr. Sci.* **2008**, *325* 503-

508.

[37] P. Majewski, B. Thierry, *Crit. Rev. Solid State* **2007**, *32*, 203-215.

[38] J.S. Kim, T.J. Yoon, B.G. Kim, S.J. Park, H.W. Kim, K.H. Lee, S.B. Park, J.K. Lee, M.H. Cho, *Toxicol. Sci.* **2006**, *89*, 338-347.

[39] X.L. Zhao, Y.L. Shi, Y.Q. Cai, S.F. Mou, *Environ. Sci. Technol.* **2008**, *42*, 1201-1206.

[40] X. Zhao, Y. Shi, T. Wang, Y. Cai, G. Jiang, *J. Chromatogr. A* **2008**, *1188*, 140-147.

[41] C. J. Tan, H. G. Chua, K. H. Ker, Y. W. Tong, *Anal. Chem.* **2008**, *80*, 683-692.

[42] W. Wu1, Q. He, C. Jiang, *Nanoscale. Res. Lett.* **2008**, *3*, 397-415.

[43] J. Kim, A. Manthiram, *J. Electrochem. Soc.* **1998**, *4*, L53-L55.

[44] K. Matsui, M. Ohgai, *J. Am. Ceram. Soc.* **1997**, *80*, 1949-1956.

[45] K.F. Purcell, J.C. Kotz, Inorganic chemistry, W. B. Saunders, Philadelphia, 1977.

[46] N. Valverde, C. Wagner, *Ber. Bunsenges. Phys. Chem.* **1976**, *80*, 330-333.

[47] Y. Zhai, J. Zhai, M. Zhou, S. Dong, *J. Mater. Chem.* **2009**, *19*, 7030-7035.

[48] A. Navrotsky, *J. inorg, nucl. Chem.* **1969**, *3*, 59-72.

[49] G. Krishnamurti, A. Violante, P. Huang, Clay Minerals 1998 33,205-212.

[50] G. Krishnamurti, A. Violante, P. M. Huang, *Clay Miner.* **1998**, *33*, 205-212.

[51] G. Schikorr, *Z. Elektrochem.* **1929**, *35*, 65-70.

[52] A. Puertas, A. Barbero, F. Nieves, L. Rull, *Langmuir* **2004**, *20*, 9861.

[53] G. Dietler, C. Aubert, D. S. Cannell, P. Wiltzius, *Phys. Rev. Lett.* **1986**, *57*, 3117.

[54] J. Zhang, R. Liu, S. Wang, Y. Xia, *Kexue Tongbao*, **1984**, 29, 1091-1096.

[55] G. Gnanaprakash, J. Philip, T. Jayakumar, B. Raj, *J. Phys. Chem. B* **2007**, *111*, 7978-7986

[56] J.-P. Jolivet, C. Froidefond, A. Pottier, C. Chaneac, S Cassaignon, E. Tronca, P. Euzen, *J. Mater. Chem.* **2004**, *14*, 3281-3288.

[57] C.-R. Lin, Y.-M. Chu, S.-C. Wang, *Mater. Lett.* **2006**, 60, 447-450

국문초록

최근 2 차 리튬 이온 전지의 사용량이 크게 증가됨에 따라 리튬의 수요 또한 크게 증가하고 있는 추세인 가운데 리튬 자원에 대한 관심이 전세계적으로 증가하고 있다. 현재 리튬의 주요 생산원은 염호로부터 얻어지는 염수, 페그마타이트 광물이며 이들은 몇몇 지역에 제한적으로 분포되어 있다. 비록 제 3 의 리튬 자원으로 알려진 해수(seawater)는 다른 자원에 비해 접근성이 좋지만 리튬이 0.15−0.2 mg/L 로 매우 낮은 농도 존재하고 있어 해수로부터 리튬 회수는 비효율적으로 여겨지고 있다. 하지만 일반 해수가 아닌 소금을 생산하기 위해서 증발 공정을 거친 함수(concentrated seawater)의 경우 비교적 높은 리튬 농도를 가져 보다 효과적인 리튬 자원으로 기대된다. 이러한 해수 기반의 리튬 자원은 리튬 이외에도 다른 금속 양이온들이 높은 농도로 용존되어 있기 때문에 리튬을 회수하기 위해서는 선택적으로 리튬을 추출할 수 있는 방법이 필요하다.

무기소재 기반의 흡착제를 사용한 흡착법은 대표적인 선택적 리튬 추출법으로서 다방면으로 연구가 진행되어 있고 리튬에 대한 선택도와 흡착능력이 높아 함수 적용에 적합한 방법으로 여겨진다. 여러 흡착제 중 망간 기반의 흡착제는 높은 성능 및 낮은 생산 비용으로 인해 가장 주요한 흡착제로 여겨지며 이는 전구체인 리튬 산화 망간의 산처리를 통해서 얻어진다. 이처럼 흡착제를 이용한 리튬 회수 공정은 수중에서 흡착제를 회수하기 위한 공정이 필요하게 되고 산업적 이용에 대한 효율을 증대시키기 위해서 여러 연구 단체에서 연구를 진행하고 있다. 과립화(granulation)나 멤브레인(membrane) 형태의 흡착제들이 수중 분리 효율을 증가시키기 위한 소재로 보고되고 있으나 이들은 제작 및 운행 비용이 높을 뿐만 아니라 유해한 물질을 사용함으로써 환경에 유해하다는 단점을 가지고 있다. 따라서 산업적 활용을 위해선 환경 친화적이고 비용적으로 효과적인 수중 분리 방법이 필요한 시점이다. 본 연구에서는 마그네타이트−리튬

산화 망간 복합체를 합성하여 이전에 연구가 많이 진행되지 않았던 자성으로 수중 분리가 가능한 리튬 흡착제의 구현화를 목표로 연구를 진행하였다. 이 복합체를 합성하기 위해서 스피넬 결정구조를 이루고 0.63 에서 1.00 의 Li/Mn 몰비를 갖는 리튬 산화 망간을 합성하였고 이를 마그네타이트가 성장할 지지체로 사용하였다. 이 리튬 산화 망간을 수산화철 ($Fe(OH)_2$) 수용액에 첨가한 후 고온에서 반응을 통해서 복합체를 합성할 수 있었다. 반응 생성물의 XRD, HR-TEM 분석을 통해서 두 결정이 생성물 한 입자 위에 존재한다는 것을 확인할 수 있었고 XPS 결과와 여러 문헌 조사를 통해서 Fe^{2+}의 산화·환원 반응을 통한 합성 메커니즘을 제안해 보았다. 이 메커니즘을 바탕으로 복합체의 자성을 최대화 시킬 수 있고 복합화 반응에서 LMO 파괴를 최소화 시킬 수 있는 조건을 확인하였고, 최적화된 조건을 바탕으로 LMO 별 복합체를 합성하였다. 이렇게 합성된 복합체들의 흡착 실험 결과 LMO-2.5 로부터 만들어진 복합체 M-LMO-2.5 가 6.84 mg/g 으로 가장 높은 흡착능을 보여주었을 뿐만 아니라 반복 실험 결과를 통해서 가장 안정적으로 흡착능을 유지하였다. 따라서 LMO-2.5 가 복합체에 가장 적합한 LMO 라는 결론을 내릴 수 있었고, 그 복합체의 산업적 적용에 대한 적합성을 평가하기 위해서 리튬에 대한 선택도 실험과 실제 함수에서의 흡착 실험을 진행하였다. 선택도 실험은 각 이온에 대한 분포 계수 (Distribution coefficient)를 측정 및 비교함에 따라 진행되었고 실험 결과 복합체는 Li^+에 대한 높은 선택도를 가지고 $Li^+ >> Mg^{2+} > Na^+ > K^+$ 의 분포 계수 크기를 가졌다. 또한 인공 리튬 용액에서뿐만 아니라 고동도의 염수인 함수에서 리튬 흡착능을 가짐으로 복합체의 산업적 적용 가능성을 보여주었다. 따라서 본 연구를 통해서 함수와 같은 높은 염도를 지닌 염수에서 리튬의 회수가 가능하고 자성으로 수중 분리가 가능한 마그네타이트-리튬 산화 망간을 성공적으로 합성할 수 있었다.